Applied Thermal Engineering 235 (2023) 121410

Contents lists available at ScienceDirect

Applied Thermal Engineering

journal homepage: www.elsevier.com/locate/apthermeng

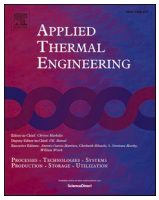

Research Paper

Parallel turbochargers for small-scale power generation

A.H. Van der Merwe, W.G. Le Roux *, E.D. Humphries

Department of Mechanical and Aeronautical Engineering, University of Pretoria, Private Bag X20, Hatfield, Pretoria 0028, South Africa

ARTICLE INFO

Keywords:
Brayton cycle
Gas turbine
Microturbine
Parallel
Turbocharger
Turbo-generator

ABSTRACT

For countries with insufficient power supply and failing power grid infrastructure, it is usually also expensive to import microturbines. Local manufacturing or local assembling in these countries is therefore an attractive solution. Off-the-shelf turbochargers used in the motor vehicle industry are readily available at relatively low costs because of large-scale manufacturing in this sector. A turbocharger can be developed into a microturbine for power generation; however, coupling a turbocharger shaft directly to a high-speed generator or gearbox can be challenging and complex due to the high speeds and high temperatures involved, as well as the limited space available on the shaft for such a conversion. The novelty of this work was to investigate the effect of mounting two off-the-shelf turbochargers in parallel, where the second turbocharger's compressor wheel is replaced with a generator. This allows for a higher pressure ratio over the power turbine. A parallel configuration may also have an advantage over a series configuration in terms of cost since the power turbine can be smaller in size. Two different parallel configurations were modelled, namely, a low-temperature turbine (LTT) and a high-temperature turbine (HTT), where the only difference was the position of the power turbine in parallel with the main shaft. Both configurations were modelled at steady state up to compressor pressure ratios of 2, with and without a recuperator, and with and without pressure losses. It was found that the recuperated LTT configuration outperformed the recuperated HTT configuration in terms of efficiency when pressure losses were introduced. Results showed that the optimum LTT combination generated up to 4.06 kW of power at 87 kPa ambient pressure, with a thermal efficiency of 13.26 %, when coupled with a 90 % effective recuperator. For the same case, the HTT configuration produced a maximum efficiency of 8.66 % with a power output of 5 kW.

1. Introduction

Globally there are about 1.1 billion people who do not have access to a national grid of which 84 % are living in rural and remote areas in developing countries [1]. The lack of power supply presents the opportunity for small-scale power generation systems to be developed [2]. Personal microturbine power generation systems may in future become as normal as owning a personal computer, according to McDonald and Rodgers [3].

To improve a microturbine's efficiency, a recuperator is usually added to transfer waste heat to the cold compressed air by decreasing the amount of combustion heat input needed to reach a specific combustion outlet temperature. Xiao et al. [4] presented a review of recuperators used for microturbines. The typical requirements for a recuperator in micro gas turbine applications include high heat transfer effectiveness and low relative pressure loss (<3 %), with cost being an important factor [4]. Dellar et al. [5] investigated the use of a sodium silicate-based sealant in the manufacturing of a microturbine recuperator in an effort to reduce recuperator costs. According to Li et al. [6], it is an important requirement of portable microturbines to be compact and if a recuperator is included, it must have a good power to weight ratio. Traverso and Massardo [7] presented an optimisation procedure for the design of recuperators for microturbine applications, which considered compactness, pressure drop and cost.

Microturbines can utilise a wide range of fuels including hydrogen [3] and can be integrated with a high-temperature solid oxide fuel cell [8], while concentrated solar power can also be used as the heat source [9,10]. The remaining exhaust heat from a microturbine can typically be applied for water heating in combined heat and power (CHP) applications [11], or for absorption chilling [12] or desalination [13]. Iora and Silva [14] presented an innovative double-shaft intercooled gas cycle for CHP using turbochargers, showing an electric efficiency of 21 % for a 50 kW biomass system. Thermal storage methods such as packed rock bed [15] and solar salts [16] have also been proposed for microturbines.

Furthermore, the automobile industry uses electrically assisted turbochargers to increase turbo response [17–19]. Noguchi et al. [20] used an ultrahigh-speed permanent magnet synchronous motor drive

* Corresponding author.
E-mail address: willem.leroux@up.ac.za (W.G. Le Roux).

https://doi.org/10.1016/j.applthermaleng.2023.121410
Received 15 February 2023; Received in revised form 20 July 2023; Accepted 18 August 2023
Available online 19 August 2023

Nomenclature

Symbols

C	Heat capacity rate [W/K]
C_p	Air isobaric specific heat [J/kgK]
d_t	Turbine exducer diameter [mm]
h	Enthalpy [J/kg]
k	Ratio of specific heats
$\dot{m}$	Mass flow rate [kg/s]
N	Rotational speed [RPM]
P	Pressure [Pa]
p	Pressure loss fraction
$\dot{Q}$	Heat transfer rate [W]
r	Pressure ratio
T	Temperature [K]
T_s	Isentropic temperature [K]
$\dot{W}$	Power [W]

Greek symbols

ε	Recuperator effectiveness
η	Efficiency

Subscripts

1–7	At state 1–7
AF	Actual flow
air	Of the air
atm	Atmosphere
avg	Average
c	Of the cold side
C	Of the compressor
CF	Corrected flow
e	Electric
g	Of the gas
GT	Of the gas turbine
h	Of the hot side
max	Maximum
min	Minimum
PT	Of the power turbine
s	Isentropic
t	Of the turbine
TOT	Total

Abbreviations

A/R	Area over radius
BSR	Blade speed ratio
CHP	Combined heat and power
EUF	Energy utilisation factor
GT	Gas turbine
HTT	High-temperature turbine
LTT	Low-temperature turbine
MGT	Micro gas turbine
PT	Power turbine
RPM	Revolutions per minute

connected to an automobile's turbocharger to produce 2.2 kW at 120 000 rpm. Lee and Hong [21] developed a high-speed surface-mounted permanent magnet synchronous motor that produced 3 kW while operating at 100 000 rpm to review the effect of eccentricity that affects vibrations. Lim et al. [22] also investigated speed response characteristics of an electrically assisted turbocharger that produced 4 kW at 150 000 rpm. Besides using an electrically assisted turbocharger to improve performance, turbochargers have also been adapted to be used as microturbine range extenders. Delta Cosworth developed a recuperated microturbine range extender (MiTRE) using a turbocharger for significant weight advantages and simple integration with an electric vehicle. Compared to other microturbines, MiTRE is inexpensive with low maintenance [23]. Metis Design Corporation (MDC) developed a unique two-spool micro gas turbine (MGT) using a turbocharger with a precombustion low-temperature power turbine connected in series with the compressor. The power output of this MGT was 40 kW with a recuperator efficiency of 60 % and an electrical efficiency of 21 % [24].

A turbocharger can be applied to complete a microturbine cycle (a Brayton power cycle) because it already consists of a turbine and compressor wheel fixed onto a common shaft [25]. Turbochargers are readily available and thus affordable [26], and have been developed for many decades to perform well at the proposed operating conditions of up to 950 °C and 1050 °C intermittently [9]. Off-the-shelf turbochargers have been proposed to act as microturbines in solar-dish Brayton cycles, in order to reduce overall cycle costs [27] while having high reliability [28]. Le Roux and Sciacovelli [9] performed an analysis on an open-cavity tubular solar receiver with integrated metallic phase-change material (PCM) for short-term thermal storage, using off-the-shelf turbochargers for power generation in a recuperated solar-dish Brayton cycle. They showed that maximum solar-to-mechanical efficiencies of 10 %–15 % could be achieved at receiver temperatures of between 900 K and 1200 K.

In recent years, many studies have been done on combining an off-the-shelf turbocharger with a generator for different applications. Maia et al. [29] adapted an automotive turbocharger to work with a generator in a compressed air energy storage system, showing that their solution could operate reliably and safely up to 70 000 rpm with a 3.5 kW load. Companies like MTT [30] developed a single-shaft recuperated microturbine generator from off-the-shelf turbochargers in an effort to reduce costs [18]. MTT's Enertwin has a net electric efficiency of 16 % and generates between 1 kW and 3.2 kW of electrical power at 100 kPa. The Enertwin also produces between 6 kW and 15.6 kW of thermal power used for cogeneration [30].

1.1. Novelty of current work

For countries with insufficient power supply and failing power grid infrastructure, it is usually also expensive to import microturbines because of various factors, such as exchange rates and importation tax. Local manufacturing or local assembling in these countries is therefore an attractive solution. Off-the-shelf turbochargers used in the motor vehicle industry are usually readily available at relatively low costs because of large-scale manufacturing in this sector. A turbocharger can therefore be developed into a microturbine for power generation; however, coupling a turbocharger shaft directly to a high-speed generator or gearbox can be challenging and complex due to the high speeds and high temperatures involved, as well as the limited space available on the shaft for such a conversion [31]. When running a second turbocharger as the power turbine, in series or in parallel with the first turbocharger, the second shaft may allow for easier modifications by having more space available, since the compressor wheel can be completely removed from the shaft.

When considering the current literature on microturbines, the generator is usually connected directly to the main shaft (single-shaft). Alternatively, the power turbine with the generator is connected in series with a main shaft (twin-shaft) as shown in Ssebabi et al. [32]; however, the pressure ratio over the power turbine is reduced, which can be detrimental for low-pressure turbomachinery such as turbochargers. The novelty of the current work is that a power turbine is connected in parallel with the main shaft and investigated as an

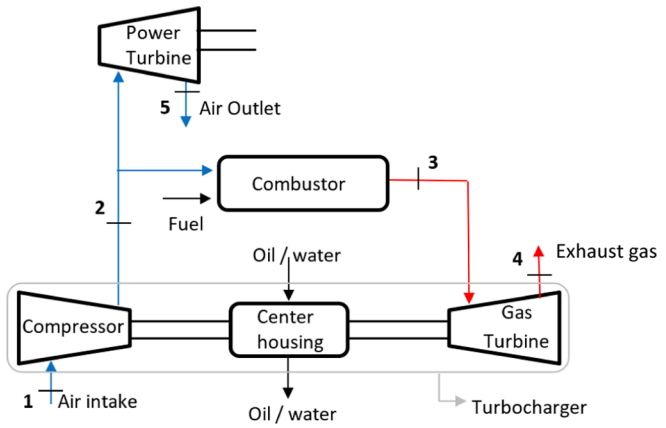

Fig. 1. LTT configuration with low-temperature PT connected in parallel before the combustion chamber.

alternative micro-turbine configuration. This allows for a higher pressure ratio over the power turbine. A parallel configuration may also have an advantage in terms of cost: since the power turbine accommodates a smaller mass flow rate it can also be smaller in size.

In this work, two different parallel-flow concepts were therefore investigated where the difference was the position of the parallel-connected power turbine. The first concept was a low-temperature turbine (LTT) connected in parallel before the combustion chamber. The second concept was a high-temperature turbine (HTT) connected in parallel with the main shaft's turbine. The low-temperature turbine eliminates the challenges faced with high-temperature connections and may also have increased life and lower maintenance costs. Seeing as pressure losses are inevitable in recuperators and combustion chambers, the LTT may have another advantage: the air flowing to the power turbine is bypassing these components with inevitable pressure losses. Therefore, a low-temperature configuration may be preferred. To the authors' knowledge, no published literature currently exists on these proposed configurations. This work therefore conceptually proposes the retrofitting of commercial turbochargers (i.e. Garrett turbochargers) for small-scale power generation, where the power turbine is connected in parallel with the main shaft.

2. Methodology

The theoretical model's objective is to find the power produced by the power turbine (PT) as well as the cycle's thermal efficiency. The theoretical analysis and the layouts of the HTT and LTT concepts are discussed in the following sections. Off-the-shelf Garrett turbochargers are considered in this work, similar to the approach followed by Le Roux and Sciacovelli [9], for both the PT and the main shaft.

2.1. LTT and HTT concepts

The layout of the LTT concept is shown in Fig. 1. The low-temperature PT is connected in parallel before the combustion chamber. The combustion chamber is positioned between the compressor and the gas turbine (the main shaft) to complete the Brayton cycle. The main turbocharger shaft does not have any external loads connected to it. The PT consumes a fraction of the compressed air coming from the compressor. Note that Garrett turbochargers use oil or water (or both) as coolant to prevent it from overheating [33].

In the high-temperature turbine (HTT) configuration, shown in Fig. 2, the high-temperature PT is connected in parallel with the main shaft's turbine, directly after the combustion chamber, and consuming a fraction of the combustion gas flow.

In both the LTT and HTT configurations, the generator on the PT is simulated as a virtual compressor (assuming another turbocharger is connected in parallel) in order to determine the speed of the PT. The concept of the virtual compressor is explained in more detail in Appendix A. The PT is coupled to the virtual compressor by having the same pressure ratio, mass flow rate, speed and power, as would be the case in a turbocharger. For the main shaft, it is assumed that the compressor wheel directly consumes the turbine wheel's power (connected on the same shaft and running at the same speed).

2.2. Compressor and turbine maps

The compressor and turbine maps of the Garrett turbochargers were available from Garrett [33]. When running the turbochargers at steady state, the operating point on the compressor map depends on the corrected mass flow rate and pressure ratio, which allows for finding the speed and the isentropic efficiency from the compressor map. For the turbine maps, a single operating line was provided by the manufacturer which coupled pressure ratio and corrected mass flow rate. When assuming a constant compressor pressure ratio, the compressor's corrected mass flow rate could therefore be calculated from the combined turbine mass flow rates that were found on their respective turbine maps (since the turbines were mounted in parallel). An image digitiser, WebPlotDigitizer was used to generate functional data in coordinate format from the original map images [34]. B-spline modelling from the built-in scipy.interpolate function in Python [35] was used to fit a curve through all of the coordinates. The data was then imported and applied for simulations by iterating through a range of compressor pressure ratios in each data set, starting from 1.4 and ending at 2. This range was chosen as an average operational range where most of the PT and GT

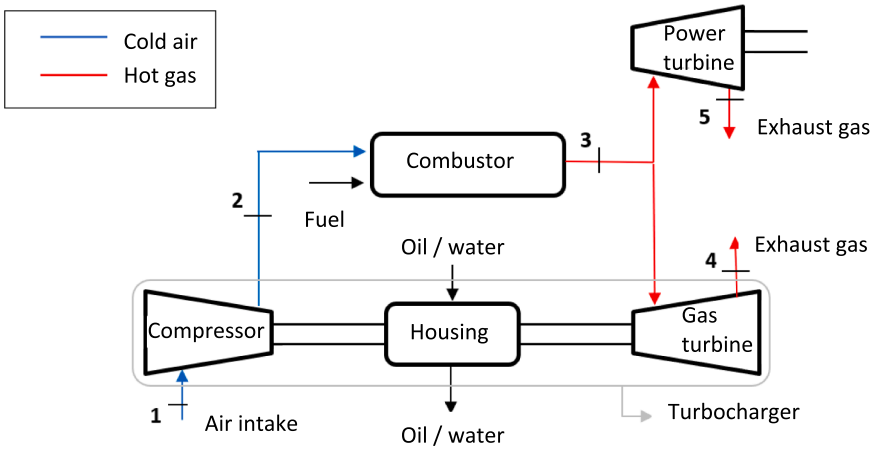

Fig. 2. HTT configuration with high-temperature PT connected in parallel with the main shaft's turbine.

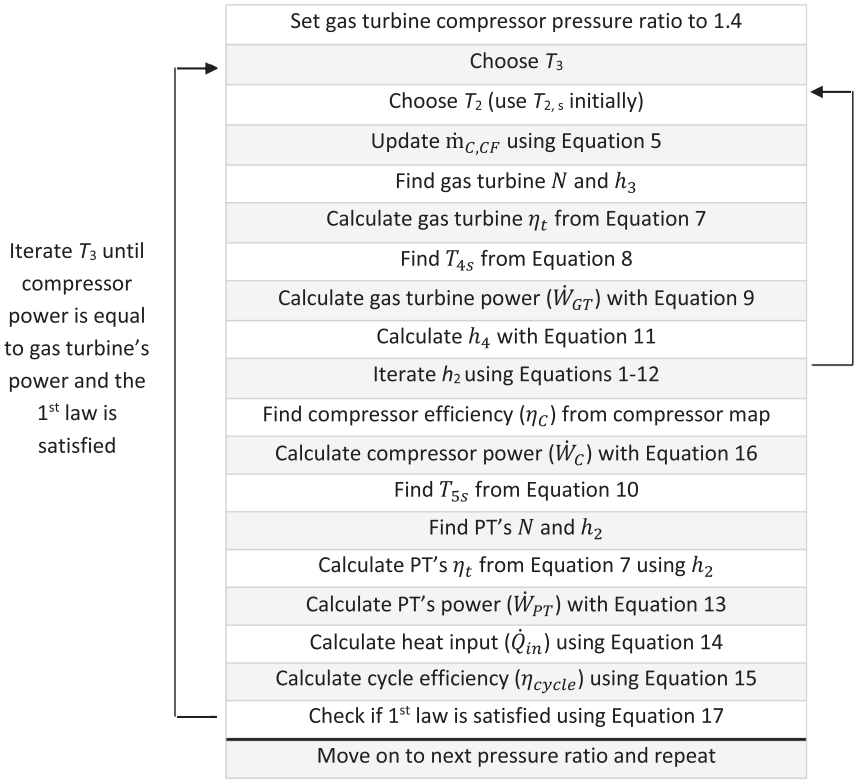

Fig. 3. Representation of the LTT iterative process used in the main model.

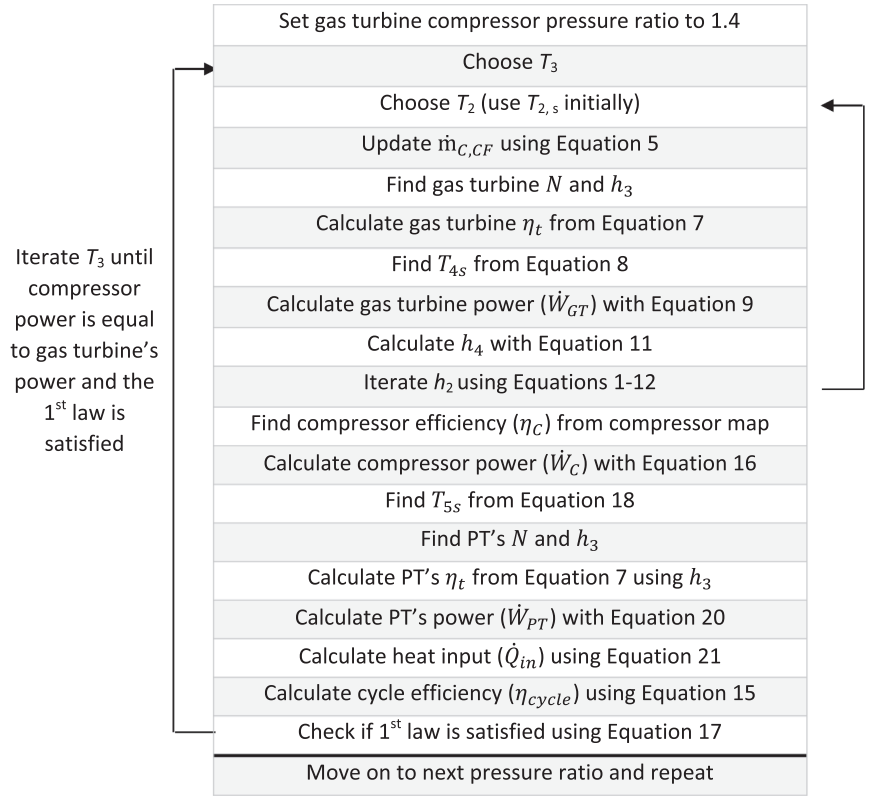

Fig. 4. Representation of the HTT iterative process used in the main model.

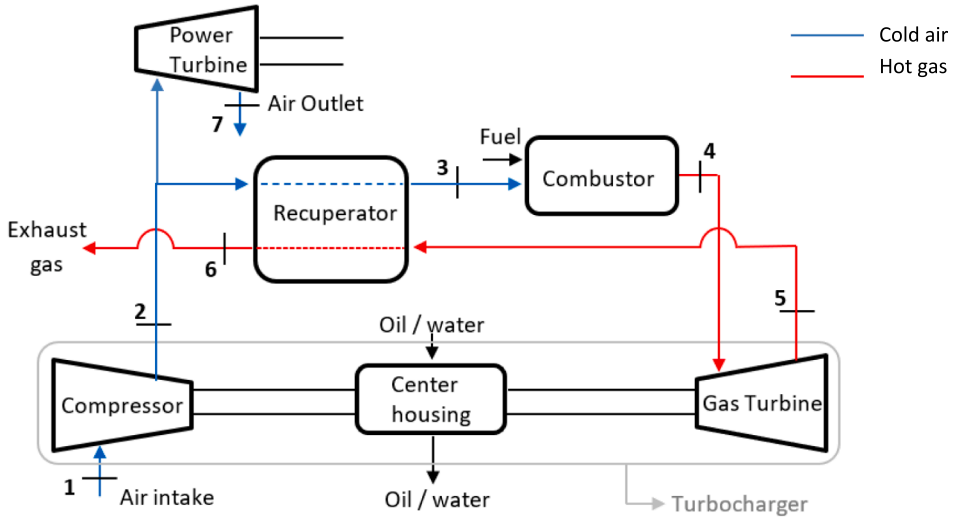

Fig. 5. Recuperated LTT configuration.

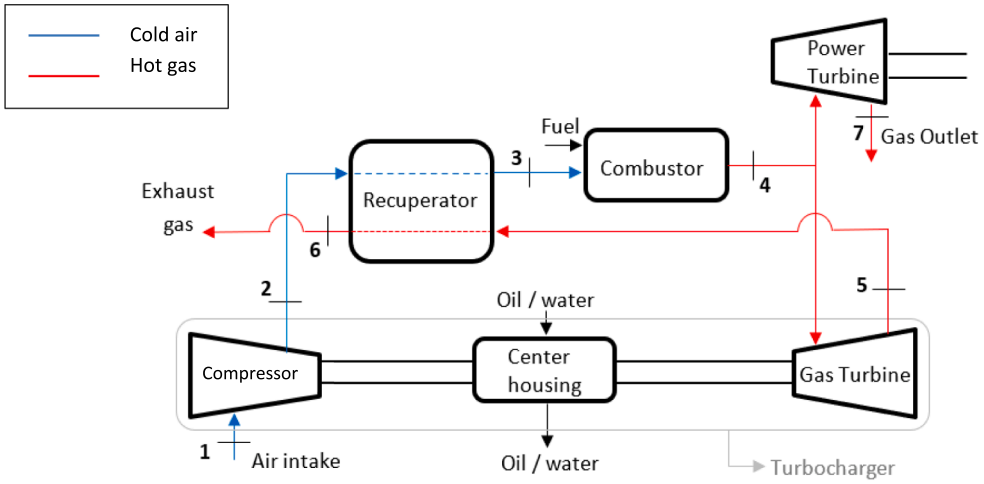

Fig. 6. Recuperated HTT configuration.

Table 1
Unrecuperated LTT cycle efficiency (in %).

Turbine used as PT	Pressure ratio	Turbocharger used as main shaft (compressor and gas turbine)			
		G25-550 (A/R = 0.49)	G25-550 (A/R = 0.72)	G25-550 (A/R = 0.92)	GT2860RS (A/R = 0.86)
GT1241 (A/R = 0.33)	**1.4**	1.63	1.51	1.29	1.36
	1.6	2.43	2.12	1.83	1.92
	1.8	3.05	2.66	2.32	2.38
	2.0	3.6	3.16	2.74	2.81
GT1544 (A/R = 0.34)	**1.4**	1.43	1.32	1.12	1.19
	1.6	2.11	1.83	1.58	1.67
	1.8	2.64	2.29	2.00	2.06
	2.0	3.10	2.71	2.35	2.42
GBC14 (A/R = 0.45)	**1.4**	*2.14*	1.99	1.74	1.77
	1.6	*3.14*	2.83	2.46	2.46
	1.8	*3.97*	3.56	3.08	3.09
	2.0	*4.64*	4.20	3.65	*3.64*
GBC17 (A/R = 0.5)	**1.4**	*2.52*	2.17	1.94	*1.91*
	1.6	*3.51*	3.10	2.74	*2.66*
	1.8	*4.38*	3.84	3.41	–
	2.0	*5.16*	*4.52*	4.00	–

Table 2
Unrecuperated LTT power output (in kW).

Turbine used as PT	Pressure ratio	Turbocharger used as main shaft (compressor and gas turbine)			
		G25-550 (A/R = 0.49)	G25-550 (A/R = 0.72)	G25-550 (A/R = 0.92)	GT2860RS (A/R = 0.86)
GT1241 (A/R = 0.33)	**1.4**	0.73	0.73	0.73	0.73
	1.6	1.31	1.31	1.32	1.32
	1.8	1.96	1.96	1.98	1.99
	2.0	2.67	2.67	2.70	2.72
GT1544 (A/R = 0.34)	**1.4**	0.63	0.63	0.63	0.63
	1.6	1.12	1.12	1.12	1.12
	1.8	1.67	1.66	1.68	1.69
	2.0	2.25	2.25	2.28	2.30
GBC14 (A/R = 0.45)	**1.4**	*1.11*	1.11	1.11	1.11
	1.6	*1.96*	1.96	1.97	1.98
	1.8	*2.95*	2.95	2.97	2.99
	2.0	*4.04*	4.05	4.08	*4.11*
GBC17 (A/R = 0.5)	**1.4**	*1.42*	1.42	1.43	*1.43*
	1.6	*2.54*	2.54	2.57	*2.58*
	1.8	*3.79*	3.81	3.85	–
	2.0	*5.17*	*5.21*	5.29	–

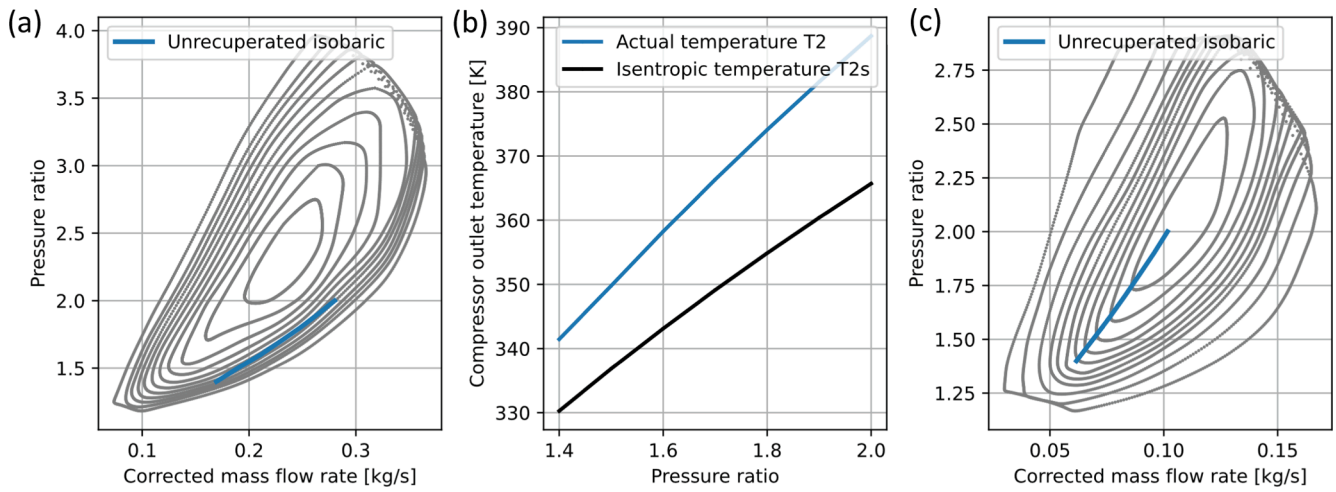

Fig. 7. Unrecuperated LTT (a) operating range and (b) compressor outlet temperature for the G25-550 (A/R = 0.92) as gasifier with (c) operating range of the GBC14 as PT (using compressor maps digitised from Garrett [33]).

Table 3
Unrecuperated LTT state properties for the G25-550 (A/R = 0.92) as main shaft with the GBC14 as PT.

Pressure ratio	State	Temperatures [K]	Pressures [kPa]	Mass flow rate [kg/s]
1.4	1	300	87	0.1540
	2	341.5	121.8	0.1540
	3	953.6	121.8	0.0980
	4	895.3	87	0.0980
	5	321.8	87	0.0560
1.6	1	300	87	0.1915
	2	358.2	139.2	0.1915
	3	970.8	139.2	0.1224
	4	889.3	87	0.1224
	5	330	87	0.0691
1.8	1	300	87	0.2252
	2	374.1	156.6	0.2252
	3	999.4	156.6	0.1441
	4	896.1	87	0.1441
	5	337.8	87	0.0811
2.0	1	300	87	0.2545
	2	388.7	174	0.2545
	3	1029	174	0.1622
	4	905.2	87	0.1622
	5	344.9	87	0.0923

combinations for both LTT and HTT configurations presented comparable results. Pressure ratios outside of this range did not necessarily present successful results. A Python programming solution solved for the RPM and compressor isentropic efficiency given the pressure ratio and the compressor corrected mass flow rate in coordinate format. To enhance the accuracy of the approximated efficiency, a fourth order polynomial function was fitted to provide interpolated efficiencies. The digitised RPM lines were used to create a fine mesh over the whole compressor map. The dataset was created by using transfinite interpolation between each RPM line. A highly accurate RPM value closest to the coordinate point was then returned.

2.3. Low-temperature turbine (LTT) analysis

The following assumptions were made:

- The properties of air at the inlet of the PT can be approximated to be the same as the outlet properties of the main shaft's compressor, assuming no heat and pressure losses in the piping section.
- All components are well insulated.

Table 4
Unrecuperated HTT cycle efficiency (in %).

Turbine used as PT	Pressure ratio	Turbocharger used as main shaft (compressor and gas turbine)			
		G25-550 (A/R = 0.49)	G25-550 (A/R = 0.72)	G25-550 (A/R = 0.92)	GT2860RS (A/R = 0.84)
GT1241 (A/R = 0.33)	**1.4**	–	2.35	1.97	2.24
	1.6	3.80	3.33	2.85	3.16
	1.8	4.35	4.12	3.62	3.93
	2.0	5.29	4.91	4.28	4.59
GT1544 (A/R = 0.34)	**1.4**	–	2.23	1.86	2.13
	1.6	–	2.68	2.67	2.99
	1.8	4.31	3.86	3.37	3.70
	2.0	5.39	4.59	4.01	4.33
GBC14 (A/R = 0.45)	**1.4**	–	2.60	2.31	2.44
	1.6	4.07	3.63	3.26	3.41
	1.8	5.13	4.50	4.09	4.25
	2.0	6.07	5.37	4.87	5.04
GBC17 (A/R = 0.5)	**1.4**	3.37	3.11	2.76	2.94
	1.6	4.78	4.33	3.89	4.12
	1.8	6.00	5.39	4.86	5.07
	2.0	7.08	6.39	5.71	5.98

Table 5
Unrecuperated HTT power output (in kW).

Turbine used as PT	Pressure ratio	Turbocharger used as main shaft (compressor and gas turbine)			
		G25-550 (A/R = 0.49)	G25-550 (A/R = 0.72)	G25-550 (A/R = 0.92)	GT2860RS (A/R = 0.84)
GT1241 (A/R = 0.33)	**1.4**	–	1.30	1.29	1.33
	1.6	1.45	2.29	2.27	2.38
	1.8	3.10	3.46	3.40	3.60
	2.0	4.34	4.66	4.62	4.95
GT1544 (A/R = 0.34)	**1.4**	–	1.22	1.21	1.25
	1.6	–	2.50	2.12	2.22
	1.8	3.68	3.17	3.11	3.32
	2.0	4.64	4.26	4.22	4.57
GBC14 (A/R = 0.45)	**1.4**	–	1.65	1.65	1.70
	1.6	3.11	2.88	2.90	2.99
	1.8	4.61	4.35	4.35	4.52
	2.0	6.34	5.97	5.99	6.25
GBC17 (A/R = 0.5)	**1.4**	2.57	2.35	2.29	2.42
	1.6	4.52	4.19	4.10	4.33
	1.8	6.66	6.21	6.09	6.50
	2.0	9.06	8.48	8.41	8.92

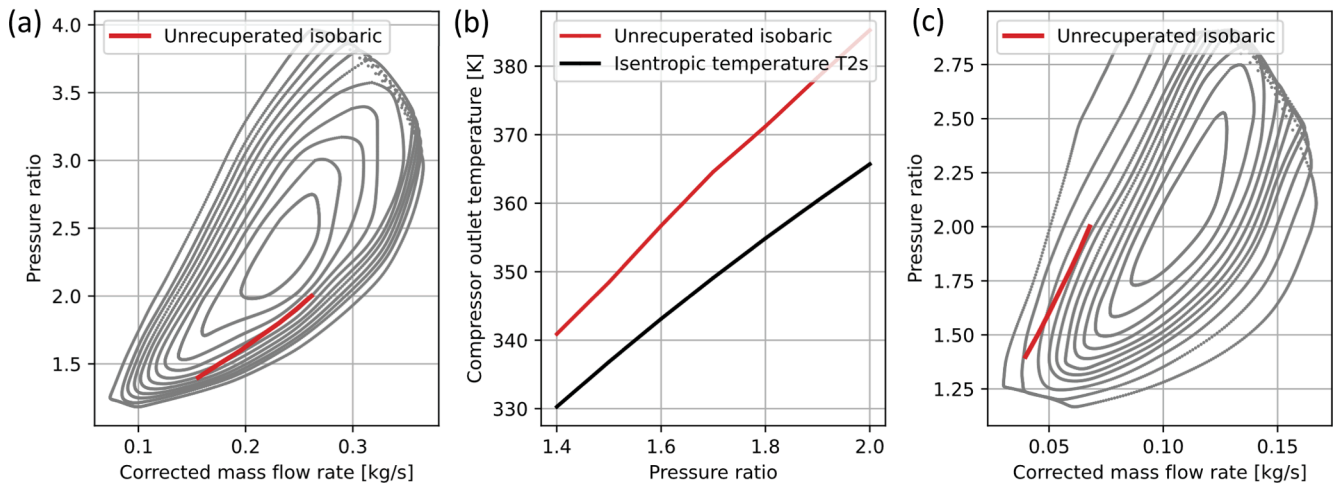

Fig. 8. Unrecuperated HTT (a) operating range and (b) compressor outlet temperature for the G25-550 (A/R = 0.92) as main shaft with (c) operating range of the GBC14 as PT (using compressor maps digitised from Garrett [33]).

Table 6
Unrecuperated HTT state properties for the G25-550 (A/R = 0.92) as main shaft with the GBC14 as PT.

Pressure ratio	State	Temperatures [K]	Pressures [kPa]	Mass flow rate [kg/s]
1.4	1	300	87	0.1416
	2	340.9	121.8	0.1416
	3	822.9	121.8	0.1416
	4	772.5	87	0.1055
	5	781.2	87	0.0361
1.6	1	300	87	0.1776
	2	356.7	139.2	0.1776
	3	832.2	139.2	0.1776
	4	762.3	87	0.1322
	5	774.1	87	0.0454
1.8	1	300	87	0.2100
	2	371.2	156.6	0.2100
	3	850.7	156.6	0.2100
	4	762.7	87	0.1562
	5	777.3	87	0.0538
2.0	1	300	87	0.2376
	2	385.3	174	0.2376
	3	874.1	174	0.2376
	4	768.9	87	0.1760
	5	786.0	87	0.0616

Table 7
Unrecuperated efficiencies (in %) with pressure losses in combustion chamber, for the G25-550 (A/R = 0.92) as the main shaft and the GBC14 as the PT.

	Pressure ratio, r_C	$dP = 0$ %	$dP = 1$ %	$dP = 2$ %	$dP = 3$ %	$dP = 4$ %
LTT	**1.4**	1.74	1.69	1.68	1.63	1.59
	1.6	2.46	2.46	2.42	2.40	2.37
	1.8	3.08	3.08	3.04	3.05	3.01
	2.0	3.65	3.62	3.62	3.58	3.59
HTT	**1.4**	2.31	2.21	2.10	1.99	1.88
	1.6	3.26	3.15	3.06	2.96	2.85
	1.8	4.09	3.99	3.88	3.79	3.68
	2.0	4.87	4.76	4.68	4.56	4.45

- The working fluid (air) is an ideal gas and the effect of adding fuel is neglected when calculating air flow rate.
- The assumed inputs for the system are as follows:
  - o $P_1 = P_{atm} = 87$ kPa,
  - o $T_1 = T_{ambient} = 300$ K,
  - o $r_C = r_{GT} = r_{PT}$ (when pressure losses were neglected),

Table 8
Unrecuperated power output with pressure losses in combustion chamber, for the G25-550 (A/R = 0.92) as the main shaft and the GBC14 as the PT.

	Pressure ratio, r_C	$dP = 0$ %	$dP = 1$ %	$dP = 2$ %	$dP = 3$ %	$dP = 4$ %
LTT	**1.4**	1.11	1.11	1.11	1.11	1.11
	1.6	1.97	1.97	1.97	1.97	1.96
	1.8	2.97	2.97	2.97	2.96	2.96
	2.0	4.08	4.08	4.08	4.08	4.07
HTT	**1.4**	1.65	1.58	1.52	1.45	1.39
	1.6	2.90	2.82	2.72	2.64	2.55
	1.8	4.35	4.24	4.14	4.01	3.91
	2.0	5.99	5.87	5.71	5.59	5.46

  - o $k_{air} = 1.4$ and $k_g = 1.333$ [36].

A high-level iteration scheme was required to solve for T_2 and T_3. For the first iteration, the compressor's pressure, P_2, and isentropic outlet temperature, T_{2s}, can be calculated from Equations (1) and (2), respectively, when considering the compressor pressure ratio as a parameter (from 1.4 to 2). Note that Equation (2) is only valid for isentropic conditions, constant C_p and for an ideal gas.

$$P_2 = P_1 \times r_C \tag{1}$$

$$T_{2,s} = T_1 \times r_C^{\left(\frac{k_{air}-1}{k_{air}}\right)} \tag{2}$$

After making an initial assumption for T_3, as well as assuming $T_2 = T_{2s}$ in the first iteration, the corrected mass flow rates for the two turbines can be read off from the digitised turbine maps. The corrected mass flow rates are the flow through the turbine/compressor adjusted to a reference pressure and temperature corresponding to ambient conditions at sea level on a standard day. Subsequently, the turbine corrected mass flow rates, in kg/s, can be converted to actual mass flow rates using Equation (3a) and (3b) based on the turbine inlet temperatures converted from Fahrenheit to Kelvin and the inlet pressures converted from pounds per square inch to Pascal [9].

The total compressor corrected mass flow rate can then be calculated by adding the two actual turbine mass flow rates (refer to Equation (4) and substituting the result into Equation (5). Note that the temperature is in Kelvin, and the pressure is in Pascal [9].

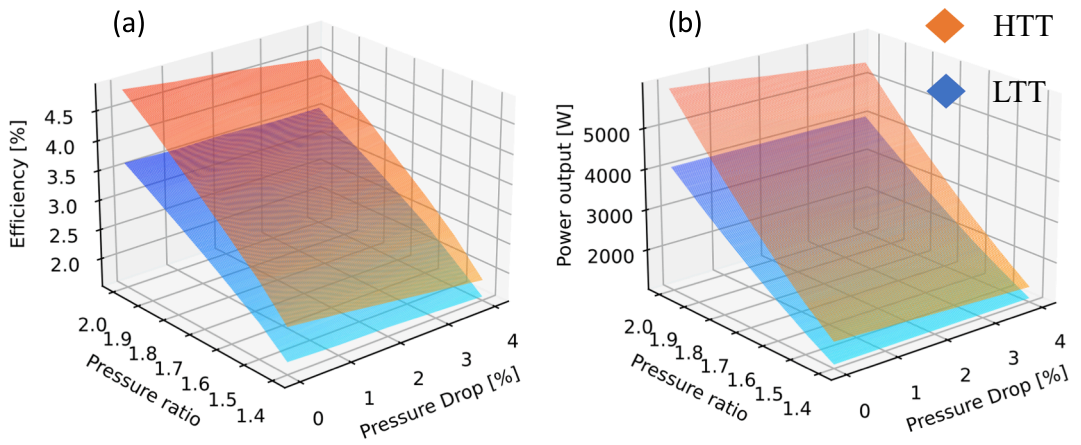

Fig. 9. Effect of pressure drop on the unrecuperated models for (a) efficiency and (b) power output, for the G25-550 (A/R = 0.92) as the main shaft and the GBC14 as the PT.

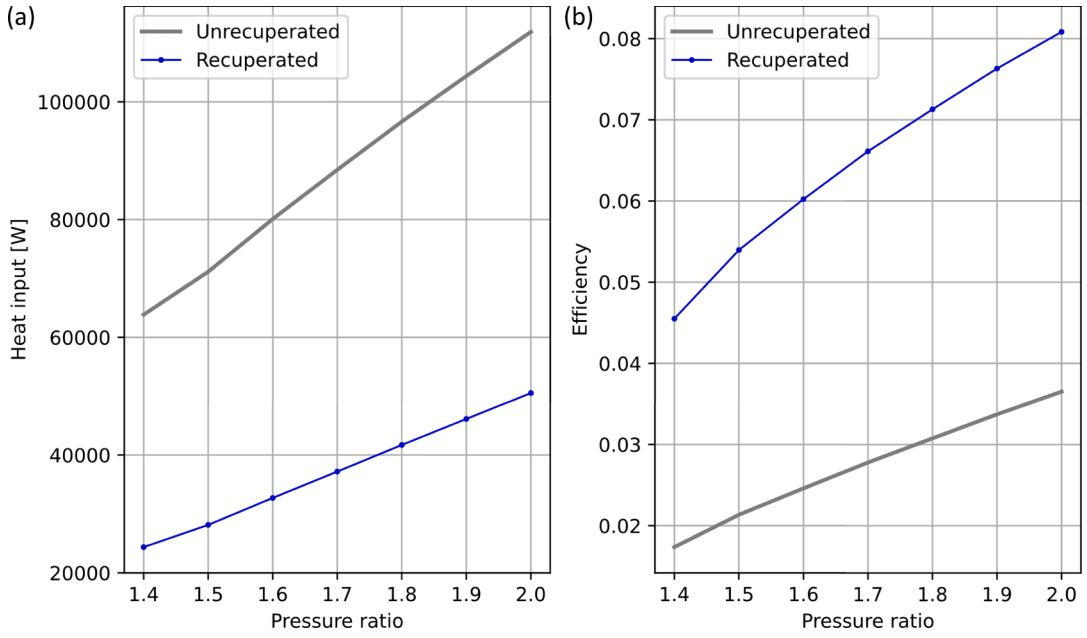

Fig. 10. The effect on (a) heat input and (b) efficiency when adding a 70 % efficient recuperator to the LTT, for the G25-550 (A/R = 0.92) as main shaft and the GBC14 as PT.

$$\dot{m}_{PT,AF} = \dot{m}_{PT,CF} \times \frac{\left(\frac{P_2}{14.7\times 6894.8}\right)}{\sqrt{\frac{((T_2-273.15)\times 1.8+492)}{519}}} \tag{3a}$$

$$\dot{m}_{GT,AF} = \dot{m}_{GT,CF} \times \frac{\left(\frac{P_3}{14.7\times 6894.8}\right)}{\sqrt{\frac{((T_3-273.15)\times 1.8+492)}{519}}} \tag{3b}$$

$$\dot{m}_{TOT} = \dot{m}_{GT,AF} + \dot{m}_{PT,AF} \tag{4}$$

$$\dot{m}_{C,CF} = \dot{m}_{TOT} \times \frac{\sqrt{\frac{(T_1-273.15)\times 1.8+492}{545}}}{\left(\frac{P_1}{13.95\times 6894.8}\right)} \tag{5}$$

$$BSR = \frac{(2\pi N/60)\times(d_t/2)}{\sqrt{2h_3\left(1-(r_{GT})^{\frac{1-k_g}{k_g}}\right)}} \tag{6}$$

$$\eta_t = \eta_{t,max} \times \left[1-\left(\frac{BSR-0.6}{0.6}\right)^2\right] \tag{7}$$

$$T_{4,s} = T_3\left(\frac{1}{r_{GT}}\right)^{\frac{k_g-1}{k_g}} \tag{8}$$

$$\dot{W}_{GT} = \eta_t \times \dot{m}_{GT,AF}\left(h_3 - h_{4,s}\right) \tag{9}$$

Since an initial value for the compressor corrected mass flow rate was calculated with Equation (5), the speed of the shaft, N, can be found from the compressor map. Subsequently, the BSR of the turbine wheel mounted on the same shaft, as well as the turbine isentropic efficiency can be found using Equations (6) and (7), respectively [9]. The turbine isentropic outlet temperature, calculated with Equation (8), allows for calculating the available gas turbine power using Equation (9).

Note that the required enthalpies in the equations above are computed from temperatures via interpolation using the CoolProp library in Python [37], similar to the ideal gas property tables in Borgnakke & Sonntag [38]. The turbine's exducer diameter, d_t in Equation (6), is available from Garrett [33] for the turbochargers that were considered.

The low-temperature PT's isentropic outlet temperature is

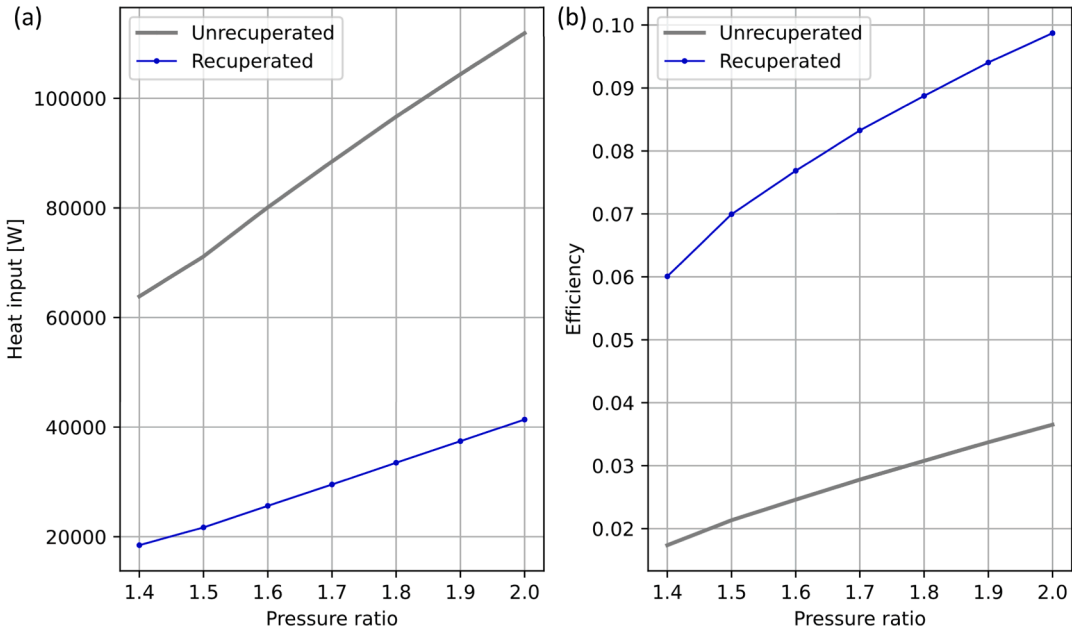

Fig. 11. The effect on (a) heat input and (b) efficiency when adding an 80 % efficient recuperator to the LTT, for G25-550 (A/R = 0.92) as main shaft and the GBC14 as PT.

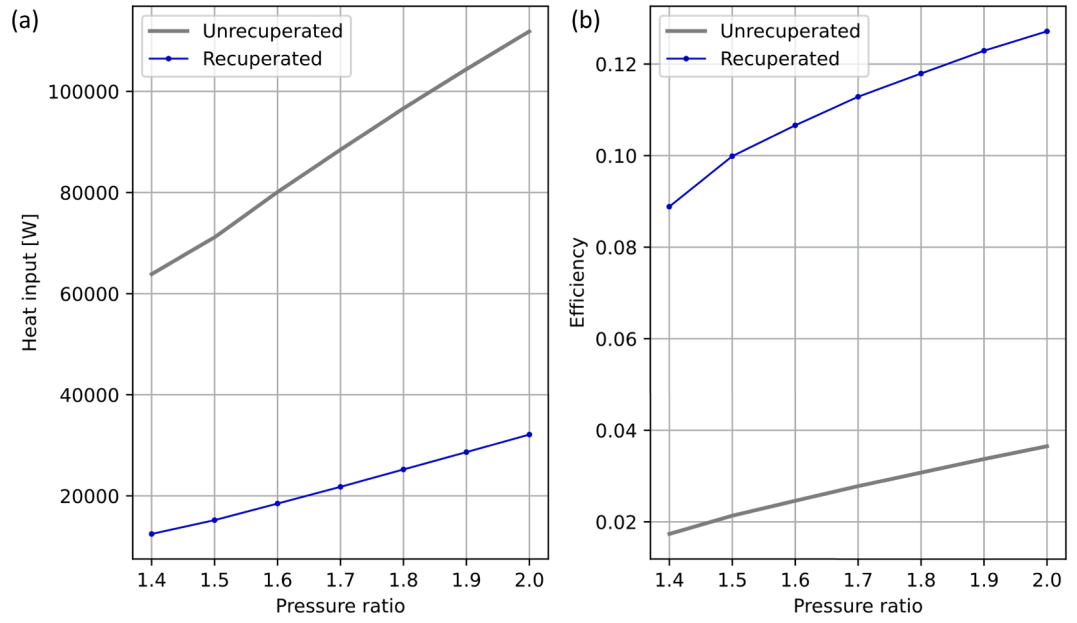

Fig. 12. The effect on (a) heat input and (b) efficiency when adding a 90 % efficient recuperator to the LTT, for G25-550 (A/R = 0.92) as main shaft and the GBC14 as PT.

dependent on the compressor outlet temperature (T_2) as shown in Equation (10) below.

$$T_{5,s} = T_2\left(\frac{1}{r_{PT}}\right)^{\frac{k_{air}-1}{k_{air}}} \tag{10}$$

The gas turbine's available power is used to calculate the actual enthalpy at the gas turbine's outlet with Equation (11).

$$h_4 = h_3 - \left(\frac{\dot{W}_{GT}}{\dot{m}_{GT,AF}}\right) \tag{11}$$

$$h_2 = \left(\frac{h_{2,s} - h_1}{\eta_C}\right) + h_1 \tag{12}$$

The compressor corrected flow in Equation (5) is updated according to the new compressor outlet enthalpy in Equation (12), which is used to find a new T_2 in Equation (3a). The iterations are continued until the outlet enthalpy (h_2) stays constant. Once the iteration scheme has been terminated, the combustion chamber heat input, the cycle efficiency, and the PT's power can be calculated. The power output of the PT is calculated using Equation (13). The combustion chamber heat input is computed with Equation (14) to solve the cycle's thermal efficiency with Equation (15).

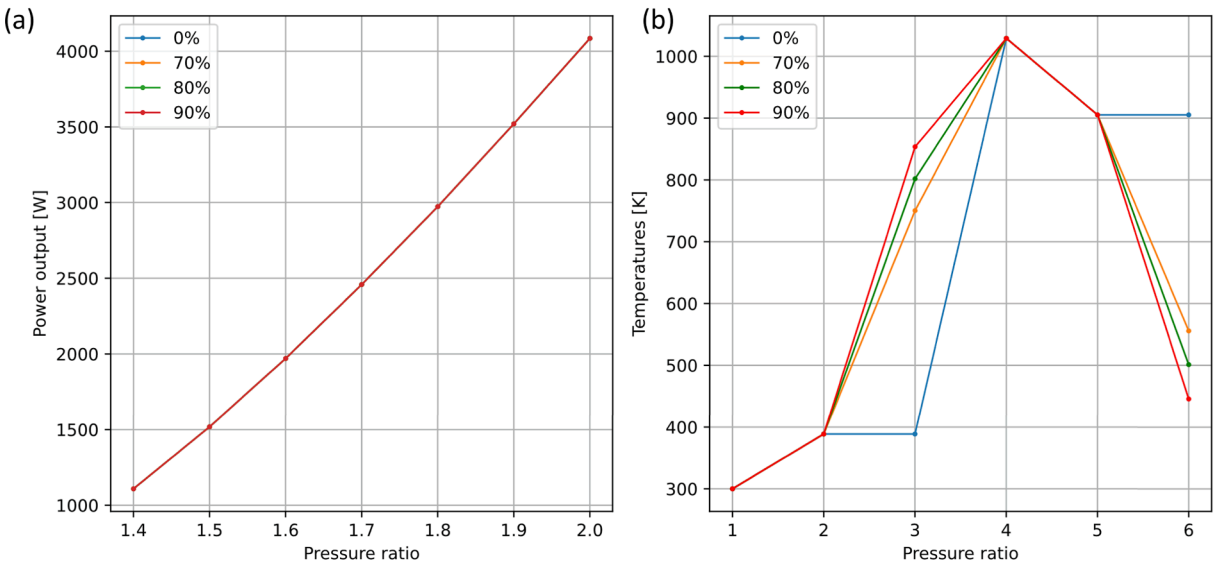

Fig. 13. Recuperated LTT's (a) power output and (b) cycle temperatures at a compressor pressure ratio of 2 for different recuperator effectiveness values, for G25-550 (A/R = 0.92) as main shaft and the GBC14 as PT.

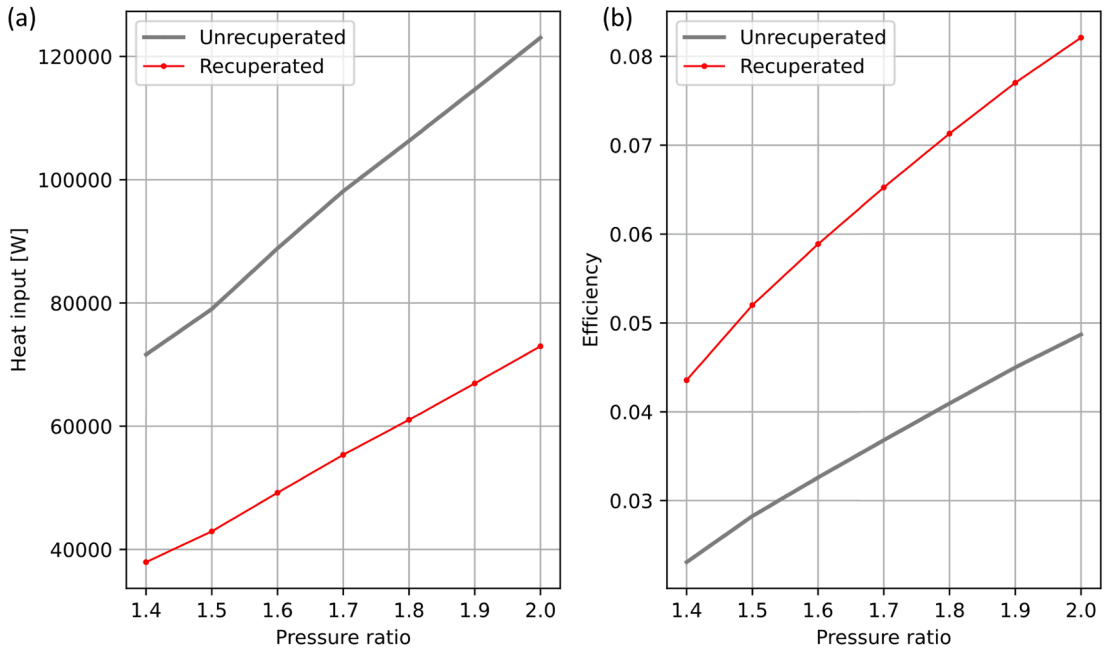

Fig. 14. The effect on (a) heat input and (b) efficiency when adding a 70 % efficient recuperator to the HTT, for the G25-550 (A/R = 0.92) as main shaft and the GBC14 as PT.

$$\dot{W}_{PT} = \eta_t \times \dot{m}_{PT,AF}\left(h_2 - h_{5,s}\right) \tag{13}$$

$$\dot{Q}_{in} = \dot{m}_{GT,AF}(h_3 - h_2) \tag{14}$$

$$\eta_{cycle} = \frac{\dot{W}_{PT}}{\dot{Q}_{in}} \tag{15}$$

The iterative model, using the *scipy.optimize.minimize* library in Python [35], optimises the temperature T_3 so that the gas turbine's power calculated with Equation (9) is equal to the compressor power calculated with Equation (16), while also adhering to the 1st law of thermodynamics applied to the boundaries of the cycle, as shown in Equation (17).

$$\dot{W}_C = \frac{\dot{W}_{C,s}}{\eta_C} = \frac{\dot{m}_{TOT} \times \left(h_{2,s} - h_1\right)}{\eta_C} \tag{16}$$

$$\dot{W}_{PT} + \dot{m}_{PT,AF}(h_5) + \dot{m}_{GT,AF}(h_4) = \dot{Q}_{in} + \dot{m}_{TOT}(h_1) \tag{17}$$

A summary of the iteration process described above is visually represented in Fig. 3.

2.4. High-temperature turbine (HTT) analysis

The theoretical analysis for the HTT is not much different from the LTT analysis. However, according to Fig. 2, the PT's inlet temperature changes throughout the model from T_2 to T_3, the mass flow rate through the combustion chamber is changed to the total air mass flow rate

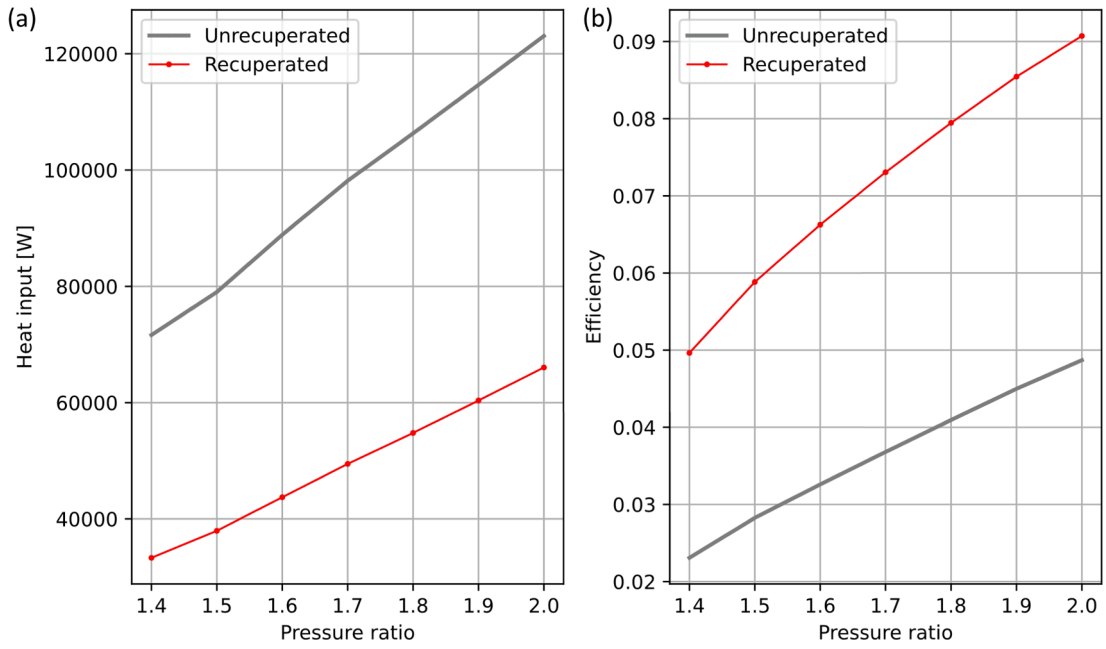

Fig. 15. The effect on (a) heat input and (b) efficiency when adding an 80 % efficient recuperator to the HTT, for the G25-550 (A/R = 0.92) as main shaft and the GBC14 as PT.

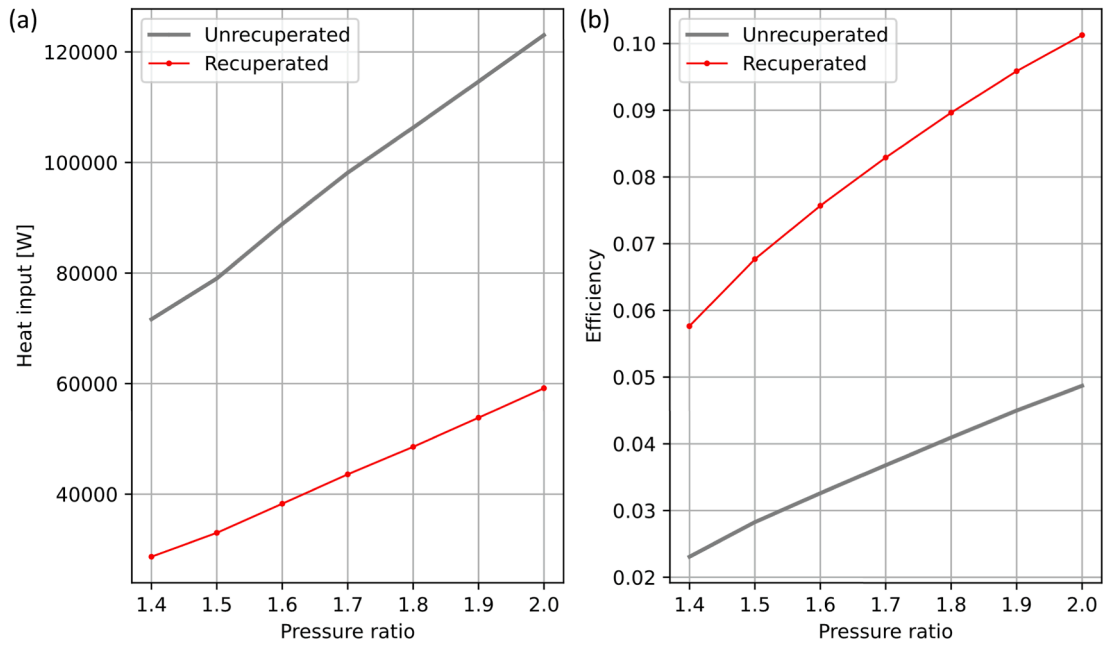

Fig. 16. The effect on (a) heat input and (b) efficiency when adding a 90 % efficient recuperator to the HTT, for the G25-550 (A/R = 0.92) as main shaft and the GBC14 as PT.

supplied by the compressor as shown in Equation (21) and lastly, the *k*-value used in Equation (10) is changed to the gas *k*-value as used for the gas turbine (see Equation (18)). Therefore, the steps discussed for the LTT are followed with minor differences. The first alteration in the model is therefore to use the combustion chamber outlet properties whenever calculating the PT's actual mass flow rate according to Equation (19). The second alteration is to use the combustion outlet enthalpy when calculating the power output of the PT with Equation (20). Fig. 4 shows the steps taken to model the HTT configuration.

$$T_{5,s} = T_3\left(\frac{1}{r_{PT}}\right)^{\frac{k_g-1}{k_g}} \tag{18}$$

$$\dot{m}_{PT,AF} = \dot{m}_{PT,CF} \times \frac{\left(\frac{P_3}{14.7\times 6894.8}\right)}{\sqrt{\frac{((T_3-273.15)\times 1.8+492)}{519}}} \tag{19}$$

$$\dot{W}_{PT} = \eta_t \times \dot{m}_{PT,AF}\left(h_3 - h_{5,s}\right) \tag{20}$$

$$\dot{Q}_{in} = \dot{m}_{TOT}(h_3 - h_2) \tag{21}$$

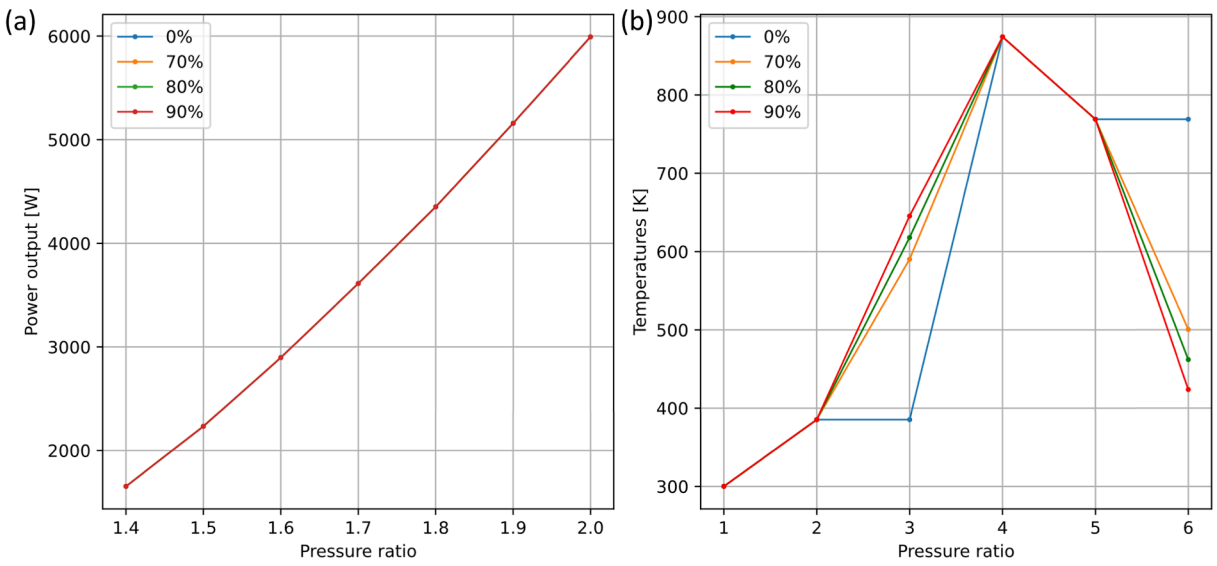

Fig. 17. HTT (a) power output and (b) cycle temperatures at a compressor pressure ratio of 2 for different recuperator efficiencies, for the G25-550 (A/R = 0.92) as main shaft and the GBC14 as PT.

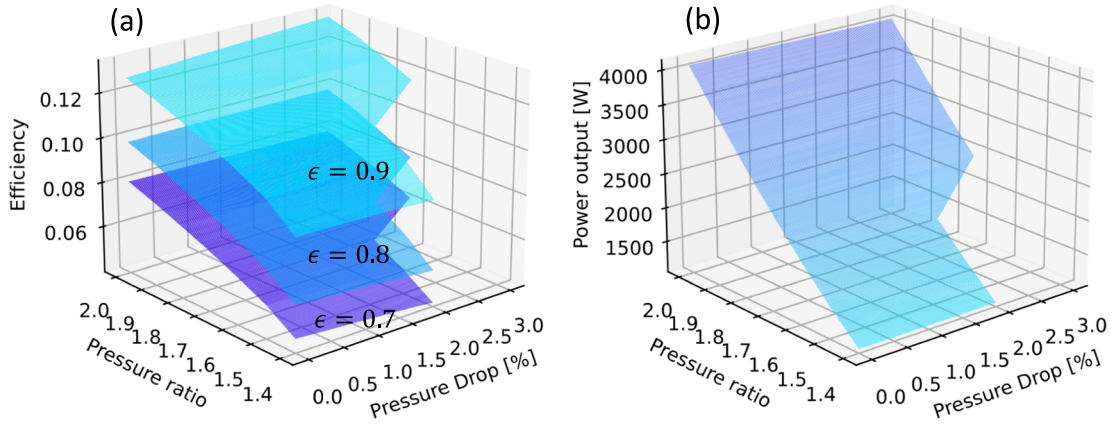

Fig. 18. (a) Efficiency and (b) power output of the recuperated LTT with pressure losses, for the G25-550 (A/R = 0.92) as main shaft and the GBC14 as PT.

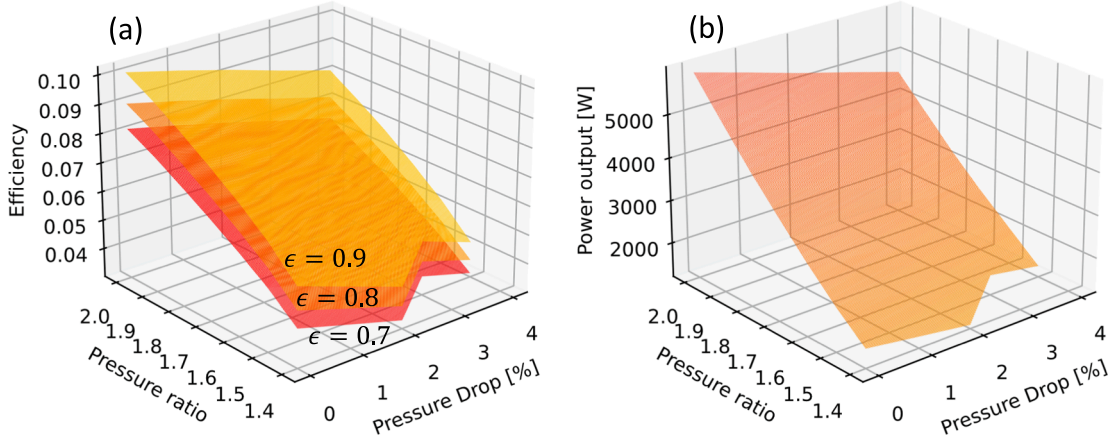

Fig. 19. (a) Efficiency and (b) power output of the recuperated HTT with pressure losses, for the G25-550 (A/R = 0.92) as main shaft and the GBC14 as PT.

2.5. Cogeneration

As mentioned in Chapter 1, the exhaust heat of a microturbine can be utilised in different applications such as cogeneration. This will increase the energy utilisation factor (EUF). In this paper, the EUF was also used as an extra verification to the model to confirm that the power generation plus the maximum rate of heat transferred to the surroundings was

Table 9
Recuperated LTT and HTT efficiencies (in %) for different pressure losses and effectiveness values, with the G25-550 (A/R = 0.92) as main shaft and the GBC14 as PT.

	Effectiveness	Pressure ratio, r_C	$dP = 0$ %	$dP = 1$ %	$dP = 2$ %	$dP = 3$ %	$dP = 4$ %
LTT	0.7	**1.4**	4.55	4.34	4.10	*3.76*	–
		1.6	6.02	5.92	5.78	5.58	*5.29*
		1.8	7.13	7.15	7.06	6.86	*6.73*
		2.0	8.08	8.04	7.97	7.89	*7.80*
	0.8	**1.4**	6.01	5.18	5.56	*5.16*	–
		1.6	7.68	7.63	7.54	7.37	*7.06*
		1.8	8.87	8.97	8.94	8.78	*8.70*
		2.0	9.87	9.90	9.90	9.88	*9.85*
	0.9	**1.4**	8.89	8.82	8.66	*8.29*	–
		1.6	10.66	10.8	10.9	10.89	*10.69*
		1.8	11.79	12.10	12.26	12.27	*12.39*
		2.0	12.71	12.91	13.09	13.26	*13.43*
HTT	0.7	**1.4**	4.36	3.82	3.30	–	–
		1.6	5.89	5.42	4.92	4.45	3.96
		1.8	7.13	6.66	6.22	5.73	5.29
		2.0	8.21	7.79	7.35	6.87	6.43
	0.8	**1.4**	4.96	4.38	3.80	–	–
		1.6	6.63	6.12	5.57	5.06	4.52
		1.8	7.95	7.45	6.97	6.45	5.97
		2.0	9.07	8.64	8.17	7.67	7.19
	0.9	**1.4**	5.76	5.11	4.46	–	–
		1.6	7.57	7.02	6.42	5.85	5.25
		1.8	8.96	8.44	7.93	7.37	6.84
		2.0	10.13	9.68	9.19	8.66	8.16

Table 10
Recuperated LTT and HTT power output (in kW) for different pressure losses, with the G25-550 (A/R = 0.92) as main shaft and the GBC14 as PT.

	Pressure ratio, r_C	$dP = 0$ %	$dP = 1$ %	$dP = 2$ %	$dP = 3$ %	$dP = 4$ %
LTT	**1.4**	1.11	1.11	1.11	*1.11*	–
	1.6	1.97	1.97	1.96	1.96	*1.96*
	1.8	2.97	2.96	2.96	2.96	*2.95*
	2.0	4.08	4.08	4.07	4.06	*4.05*
HTT	**1.4**	1.65	1.47	1.29	–	–
	1.6	2.90	2.67	2.46	2.24	2.04
	1.8	4.35	4.07	3.80	3.53	3.25
	2.0	5.99	5.65	5.29	4.97	4.63

Table 11
Recuperated LTT and HTT parameters for the G25-550 (A/R = 0.92) as main shaft and the GBC14 as the PT at steady state (at a compressor pressure ratio of 2).

Parameter	LTT	HTT
Ambient temperature [K]	300	300
Ambient pressure [kPa]	87	87
Compressor pressure ratio	2	2
Gas turbine exhaust temperature (after the recuperator) [K]	460	430
Gas turbine actual mass flow rate [kg/s]	0.140	0.155
Maximum water heating capacity of the gas turbine exhaust [kW]	22.6	20.4
Power turbine exhaust temperature [K]	342	864
Power turbine actual mass flow rate [kg/s]	0.0927	0.0536
Maximum water heating capacity of the power turbine exhaust [kW]	3.92	32.0
Total maximum water heating capacity [kW]	26.6	52.4
Power output [kW]	4.06	4.97
Combustion heat input rate [kW]	30.6	57.3
EUF	1	1

equal to the total rate of heat input into the system (an EUF = 1). Therefore, Equation (15) was modified to include the exhaust heat from both turbines to calculate the EUF with Equation (22).

$$EUF = \frac{\dot{W}_{PT} + \dot{m}_{GT,AF} \times (h_4 - h_1) + \dot{m}_{PT} \times (h_5 - h_1)}{\dot{Q}_{in}} \quad (22)$$

2.6. Recuperation

For additional comparison between the LTT and HTT and to improve the cycle efficiency, the addition of a counterflow recuperator was also considered. A recuperator will increase the combustion chamber's inlet temperature. Two nodes are added to the theoretical model at the recuperator outlets. The outlet temperatures of the recuperator depend largely on the recuperator effectiveness. The recuperator effectiveness is specified as a range of constant values and modelled as an array, [0.7, 0.8, 0.9]. When heat is added to the cold air in the recuperator, less heat is required from the combustion chamber to get to the required combustion outlet temperature. From Equation (15) it is evident that the cycle's efficiency will increase as the heat input decreases. The recuperated models are explained in the sub-sections below.

2.6.1. Recuperated LTT

For the recuperated LTT, heat is added to the cold air before it enters the combustion chamber as shown in the layout in Fig. 5.

Equations (23) to (30) represent the equations added to the unrecuperated model after the iteration scheme but before calculating the heat input into the system. In the recuperated LTT layout shown in Fig. 5, the mass flow rate for the cold and hot side of the recuperator are the same.

$$C_c = \dot{m}_{GT,AF} \times C_{p,avg(T_2,T_3)} \quad (23)$$

$$C_h = \dot{m}_{GT,AF} \times C_{p,avg(T_5,T_6)} \quad (24)$$

$$C_{min} = \min(C_c, C_h) \quad (25)$$

After the heat capacity rates have been calculated using Equations (23)–(25), the heat transfer rate can be calculated using Equation (26), assuming a recuperator with no heat loss to the environment. For calculating the maximum heat transfer rate in the equations below, the minimum heat capacity rate is used [39]. The C_p value is evaluated at the average temperature.

$$\dot{Q} = C_c \times (T_3 - T_2) = C_h \times (T_5 - T_6) \quad (26)$$

$$\dot{Q}_{max} = C_{min} \times (T_5 - T_2) \quad (27)$$

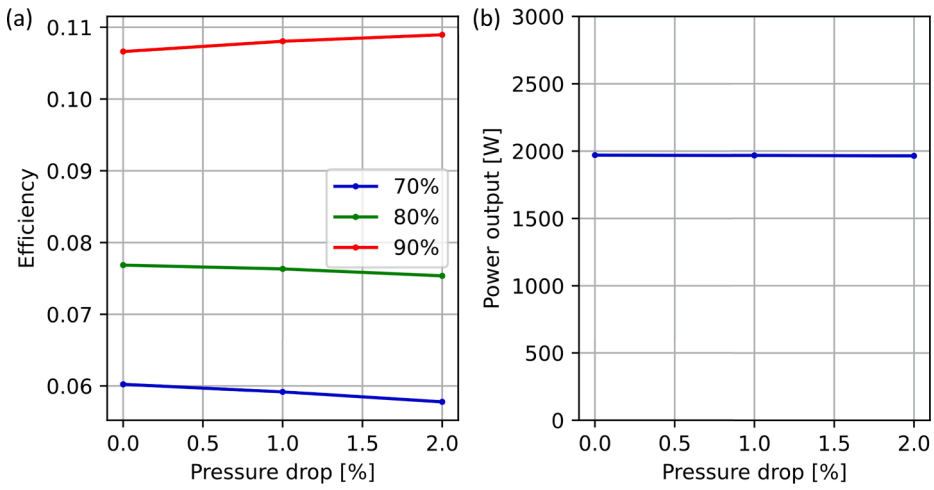

Fig. 20. Recuperated LTT (a) efficiency and (b) power output for different pressure losses and effectiveness values at $r_C = 1.6$, for the G25-550 (A/R = 0.92) as main shaft and the GBC14 as PT.

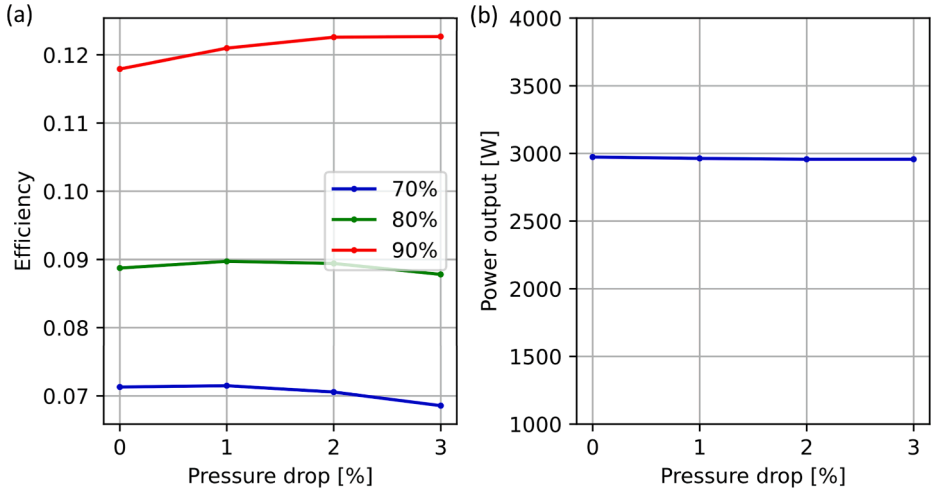

Fig. 21. Recuperated LTT (a) efficiency and (b) power output for different pressure losses and effectiveness values at $r_C = 1.8$, for the G25-550 (A/R = 0.92) as main shaft and the GBC14 as PT.

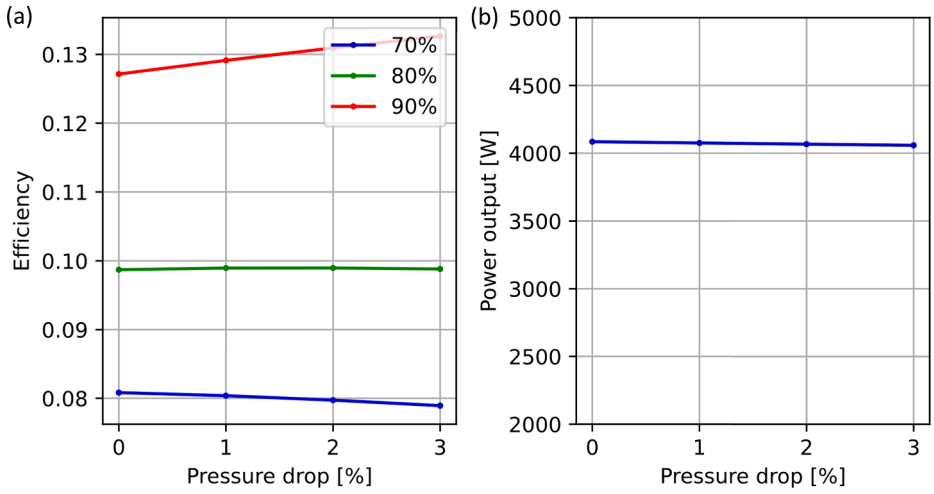

Fig. 22. Recuperated LTT (a) efficiency and (b) power output for different pressure losses and effectiveness values at $r_C = 2.0$, for the G25-550 (A/R = 0.92) as main shaft and the GBC14 as PT.

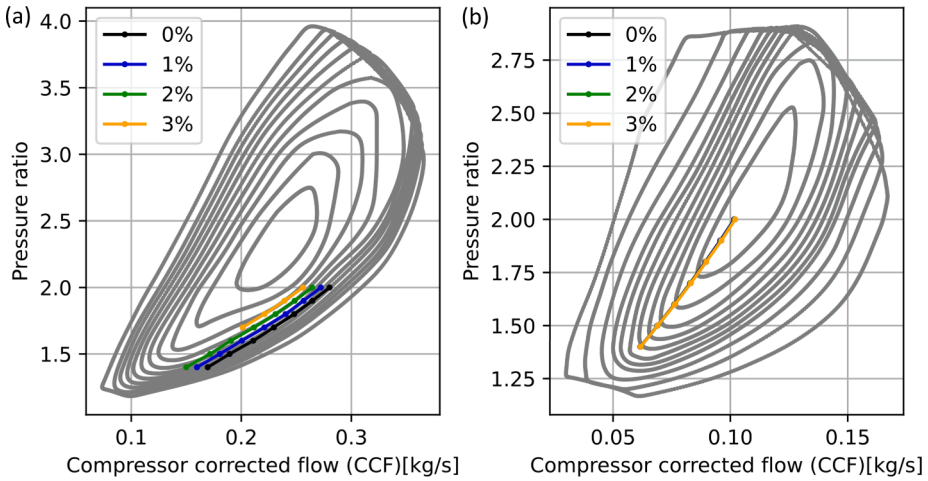

Fig. 23. LTT operating range for the (a) G25-550 with A/R = 0.92 as main shaft and (b) GBC14 as PT.

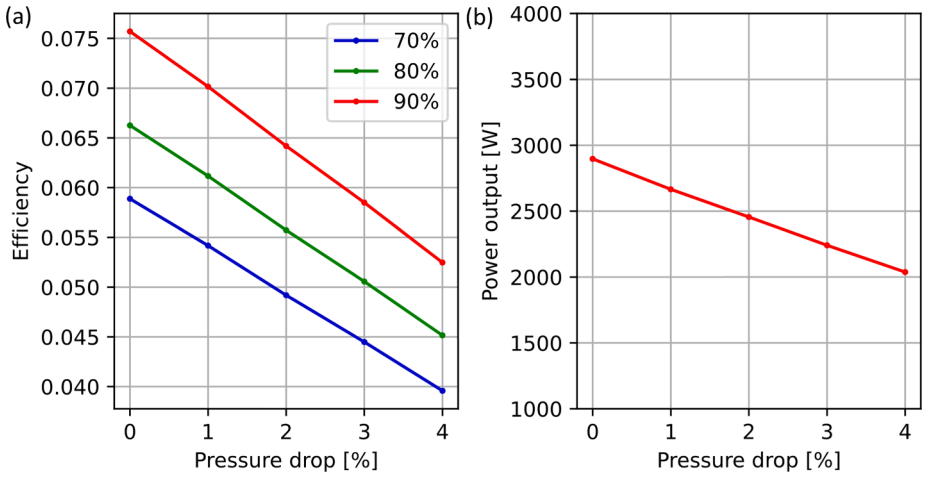

Fig. 24. Recuperated HTT (a) efficiency and (b) power output for different pressure losses and effectiveness values at $r_C = 1.6$, for the G25-550 (A/R = 0.92) as main shaft and the GBC14 as PT.

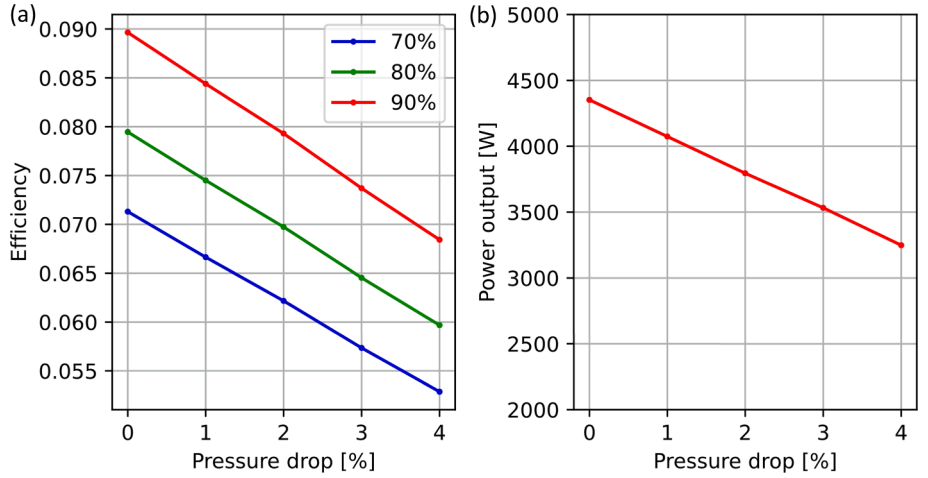

Fig. 25. Recuperated HTT (a) efficiency and (b) power output for different pressure losses and effectiveness values at $r_C = 1.8$, for the G25-550 (A/R = 0.92) as main shaft and the GBC14 as PT.

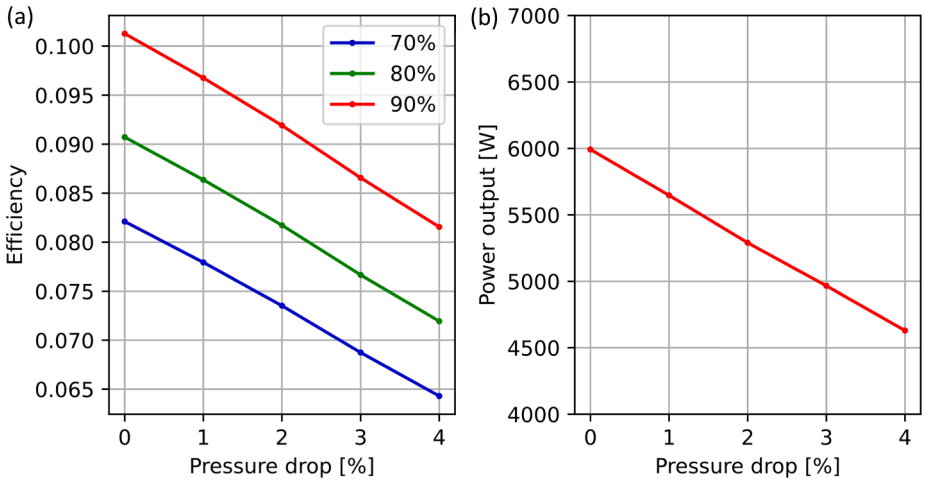

Fig. 26. Recuperated HTT (a) efficiency and (b) power output for different pressure losses and effectiveness values at $r_C = 2.0$, for the G25-550 (A/R = 0.92) as main shaft and the GBC14 as PT.

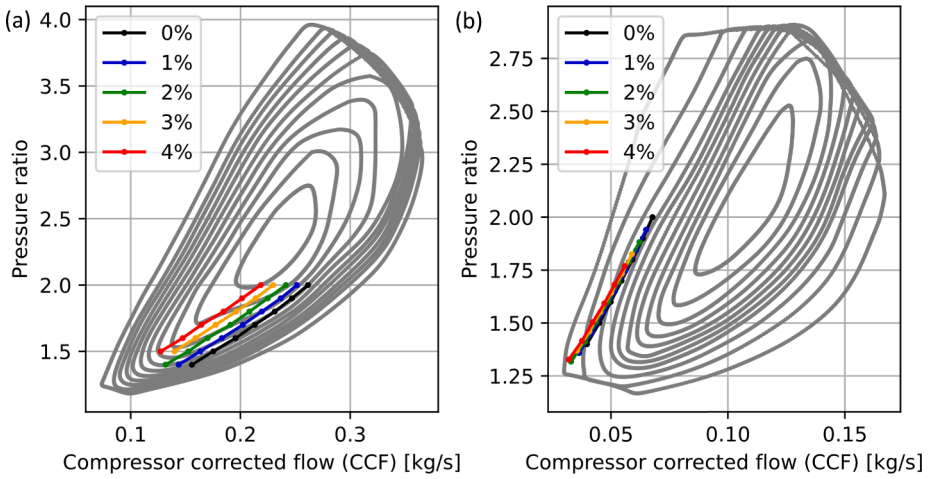

Fig. 27. HTT operating range for the (a) G25-550 with A/R = 0.92 as main shaft and (b) GBC14 as PT.

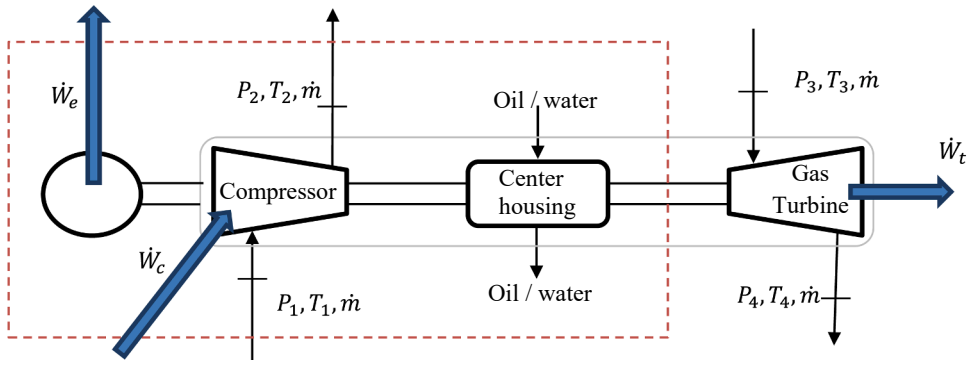

Fig. A1. Equivalence model.

$$\dot{Q} = \varepsilon \times \dot{Q}_{max} \tag{28}$$

Equation (29) is found by simultaneously solving Equations (27) and (28). This is used to calculate the total heat input into the system with Equation (30).

$$T_3 = T_2 + \varepsilon \times \left(\frac{C_{min}}{C_c}\right) \times (T_5 - T_2) \tag{29}$$

$$\dot{Q}_{in} = \dot{m}_{GT,AF} \times (h_4 - h_3) \tag{30}$$

The cycle efficiency can be updated with Equation (15) using the heat input into the recuperated LTT system. Equation (26) is used to derive Equation (31) for finding the recuperator hot-side outlet temperature.

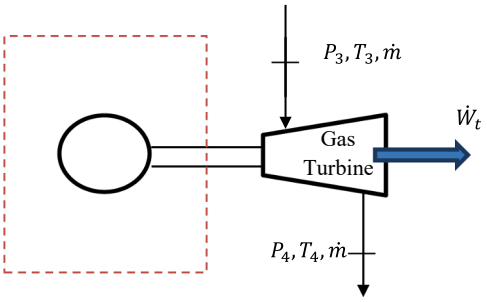

Fig. A2. Simplified equivalence model.

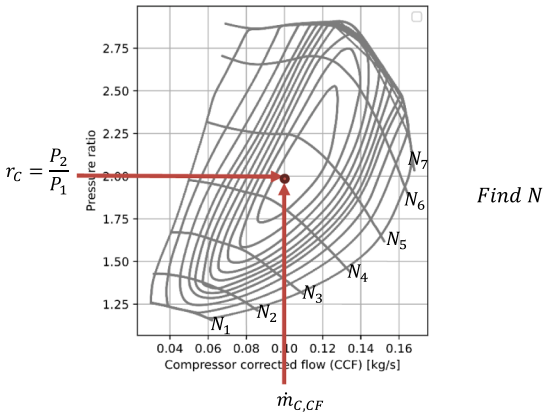

Fig. A3. Operating point on the compressor map [33].

Table B1
Properties of the different turbochargers [33].

Turbocharger	Turbine exducer diameter [m]	Maximum turbine efficiency [-]
GT1241	0.0355	0.65
GT1544	0.0422	0.62
GBC14	0.036	0.65 *(assumed)*
GBC17	0.04	0.65 *(assumed)*
G25-550	0.049	0.76
GT2860RS	0.0538	0.72

Table B2
Compatibility of the different turbochargers (for the LTT, recuperated and with pressure losses).

Turbochargers used as power turbines	Turbochargers used as main shafts (compressor and gas turbine)			
	G25-550 (A/R = 0.49)	G25-550 (A/R = 0.72)	G25-550 (A/R = 0.92)	GT2860RS (A/R = 0.84)
GT1241 (A/R = 0.33)	Semi-compatible	OK	OK	OK
GT1544 (A/R = 0.34)	Semi-compatible	OK	OK	OK
GBC14 (A/R = 0.45)	$T_3 > 950$ °C	OK	OK	$T_3 > 950$ °C
GBC17 (A/R = 0.5)	$T_3 > 950$ °C	$T_3 > 950$ °C	Semi-compatible	$T_3 > 950$ °C

$$h_6 = h_5 - \frac{\dot{m}_{GT}(h_3 - h_2)}{\dot{m}_{GT,AF}} \tag{31}$$

2.6.2. Recuperated HTT

For the recuperated HTT layout, the same methodology is used as for the LTT. However, the full mass flow rate is evident on the cold side of the recuperator (see Fig. 6), not just a fraction thereof. This results in Equations (23) and (30) using total mass flow rate instead of the gas turbine's fraction of the total mass flow rate. These equations are updated accordingly as shown in Equations (32) to (33).

$$C_c = \dot{m}_{TOT} \times C_{p,avg(T_2,T_3)} \tag{32}$$

$$\dot{Q}_{in} = \dot{m}_{TOT} \times (h_4 - h_3) \tag{33}$$

For the LTT, in Equation (29), the cold outlet temperature of the recuperator can be solved for without an iterative scheme, due to C_{min} being equal to C_c. For the HTT, however, C_{min} is equal to C_h. Therefore, Equation (34) is first used to solve the recuperator's hot side outlet temperature. The outlet enthalpy of the cold side of the recuperator can then be found with Equation (35).

$$T_6 = T_5 - \varepsilon \times \left(\frac{C_{min}}{C_h}\right) \times (T_5 - T_2) \tag{34}$$

$$h_3 = h_2 + \frac{\dot{m}_{GT,AF}(h_5 - h_6)}{\dot{m}_{TOT}} \tag{35}$$

2.7. Pressure losses

Both the LTT and HTT configurations were also modelled with a range of constant pressure losses in the recuperator (for both the hot and the cold side) and in the combustion chamber. The pressure losses that were considered in each component are $p = [0, 0.01, 0.02, 0.03, 0.04]$. For the unrecuperated models, only the combustion outlet pressure was updated according to Equation (36) (referring to the unrecuperated systems shown in Fig. 1 and Fig. 2).

$$P_3 = P_2(1 - p) \tag{36}$$

Note that the recuperator will not have a direct effect on the power output of the system when $p = 0$ %, but it will still directly influence the thermal efficiency. On the contrary, when $p > 0$ %, the recuperator will have a direct effect on the power output of the system as well as on the thermal efficiency. To simulate the pressure losses of a recuperated model and to calculate the power output of the system, extra pressure losses were therefore first introduced into the unrecuperated models, but with a recuperator effectiveness of 0 %. The pressure loss in the cold side of the recuperator, in the hot side of the recuperator and in the combustion chamber were therefore applied by multiplying the inlet pressure with $(1 - p)$. The recuperator effectiveness was then implemented afterwards, once the thermal efficiency of the cycle had been calculated. This was done to save simulation time because the recuperator effectiveness only affected the heat input into the system.

Note that, in the unrecuperated cycles with only combustion pressure losses, the gas turbine expands the air to atmospheric pressure with a pressure ratio of r_{GT}, while in the recuperated cycles, the gas turbine has a back pressure at its outlet due to the pressure loss in the recuperator's hot side. Consequently, the pressure ratio over the gas turbine (in the recuperated cycles) was calculated using Equation (37), since $P_5 = \frac{P_6}{(1-p)}$ and assuming $P_1 = P_6$.

$$r_{GT} = \frac{P_4}{\left(\frac{P_6}{1-p}\right)} \tag{37}$$

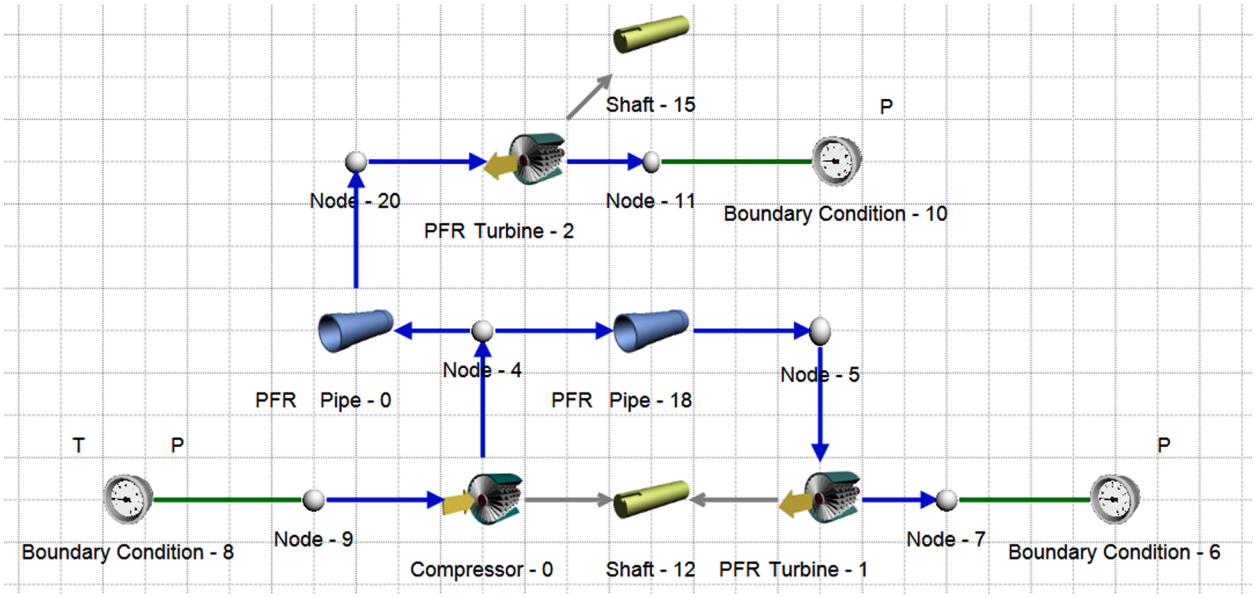

Fig. C1. Flownex layout diagram for an unrecuperated LTT system.

Table C1
Flownex and Python temperatures and pressures at each state for an unrecuperated LTT system (without pressure losses) with main shaft at 96 100 rpm and 63.86 kW heat input rate (using the G25-550 with A/R = 0.92 as the main shaft and GBC14 as the power turbine).

State	Temperature [K]			Pressure [kPa]		
	Flownex	Analytical model	Difference [%]	Flownex	Analytical model	Difference [%]
1	300	300	0	87	87	0
2	340.5	341.5	0.3	121.3	121.8	0.4
3	962.7	953.6	1.0	121.3	121.8	0.4
4	909.1	895.3	1.5	87	87	0
5	320.8	321.8	0.3	87	87	0

Table C2
Flownex and Python results for an unrecuperated LTT system (without pressure losses) with the main shaft at 96 100 rpm and 63.86 kW heat input rate (using the G25-550 with A/R = 0.92 as the main shaft and GBC14 as the power turbine).

	Pressure ratio	Power output [W]	Efficiency [%]	PT mass flow rate [kg/s]	GT mass flow rate [kg/s]
Flownex	1.394	1097	1.72	0.0556	0.0962
Analytical model	1.4	1111	1.74	0.056	0.098
Difference [%]	0.4	1.0	1.1	0	1.4

3. Results

The analytical model considered a range of Garrett turbochargers in different combinations (in total, 552 different combinations were considered) to find the turbocharger combinations with the best performance. The Garrett turbochargers that were identified for further consideration were the GT1241, GT1544, GBC14, GBC17, G25-550R and the GT2860RS [33]. The turbocharger parameters are summarised in Appendix B. The GBC14 and GBC17 were assumed to have similar performance as similarly sized turbine wheels since the maximum turbine efficiencies were not available from the manufacturer. These Garrett turbochargers were used in different main shaft and PT combinations. Even though in a physical setup only the turbocharger's turbine is required for the PT (to be connected to a generator directly or via a gearbox), the turbocharger's compressor map was still implemented to determine the turbine's RPM for the theoretical model (since speed lines are not included in Garrett's turbine maps – see Appendix A).

Table D1
Unrecuperated LTT system (without pressure losses) Flownex results at 87 kPa ambient pressure (using the G25-550 with A/R = 0.92 as the main shaft and GBC14 as the power turbine) - using the same shaft speeds and heat input rates that were found from the analytical model.

Pressure ratio	Power (W)	Main shaft speed (RPM)	Heat input rate (W)	PT mass flow rate (kg/s)	GT mass flow rate (kg/s)	Turbine inlet temperature (K)
1.394	1097	96 100	63 859	0.0556	0.0962	962.7
1.490	1498	104 800	71 151	0.062	0.108	966.2
1.591	1940	113 900	80 105	0.0685	0.12	979
1.689	2405	121 225	88 464	0.0754	0.131	998.3
1.784	2836	128 250	96 650	0.08	0.142	1007.5
1.882	3311	134 600	104 373	0.0861	0.15	1023.9
1.981	3819	140 625	111 876	0.0917	0.159	1039.5

Table D2
Effect of ambient pressure on the unrecuperated LTT system (without pressure losses) at 96 100 rpm and 63.86 kW heat input rate (using the G25-550 with A/R = 0.92 as the main shaft and GBC14 as the power turbine).

Ambient pressure (kPa)	Pressure ratio	Power (W)	PT mass flow rate (kg/s)	GT mass flow rate (kg/s)	GT inlet temperature (K)
87	1.394	1097	0.0556	0.0962	962.73
100	1.382	1197	0.0626	0.115	867.79

3.1. Without recuperator

3.1.1. Unrecuperated LTT results

The unrecuperated results for the LTT configuration without any pressure losses are shown in Tables 1 and 2 for the thermal efficiency and power output respectively.

When the combustion outlet temperature is greater than 950 °C, the values are displayed in italics. The combinations are also assumed to not be compatible when the operating point is outside either the main shaft's compressor map or the PT's compressor map. The operating range of the main shaft's compressor, the outlet temperature of the compressor and the operating range of the PT (visualised using the virtual compressor map) are shown in Fig. 7, where the G25-550 (A/R = 0.92) is used as main shaft and the GBC14 (A/R = 0.45) as the PT. For this same combination, the state properties at an ambient temperature of T_1 = 300 K and ambient pressure of P_1 = 87 kPa, with numbers corresponding to Fig. 1, are shown in Table 3 (see model verification in Appendix C and additional Flownex results in Appendix D).

3.1.2. Unrecuperated HTT results

The same combinations used for the LTT configuration are used for the unrecuperated HTT configuration. The efficiency and power output are presented in Tables 4 and 5 respectively for no pressure losses in the system. The HTT analysis is also for a range of pressure ratios of between 1.4 and 2 so that the HTT results can be compared to the LTT results.

The HTT configuration has more compatible combinations with acceptable combustion outlet temperatures. The amount of power produced and the cycle efficiencies are higher. The operating range of the main shaft's compressor, the outlet temperature of the compressor and the operating range of the PT (visualised using the virtual compressor map) are shown in Fig. 8, where the G25-550 (A/R = 0.92) is used as main shaft and the GBC14 (A/R = 0.45) as the PT. Fig. 8-a and Fig. 8-c is therefore a visual representation of the operating range of the main shaft's compressor and of the virtual compressor connected to the PT respectively.

For the combination shown in Fig. 8 where the G25-550 (A/R = 0.92) is used as the main shaft and the GBC14 (A/R = 0.45) as the PT, the state properties at an ambient temperature of T_1 = 300 K and ambient pressure of P_1 = 87 kPa, with numbers corresponding to Fig. 2, are shown in Table 6.

3.1.3. Effect of pressure loss in the combustion chamber (unrecuperated)

The unrecuperated cycle results presented above did not have any pressure losses, meaning that $P_2 = P_3$. The combustion chamber was modelled with a constant pressure drop percentage from 0 % to 4 %. The combination presenting the best performance was for the G25-550 (A/R = 0.92) as the main shaft and the GBC14 as the PT. The results are tabulated in Tables 7 and 8 and visually represented in Fig. 9 at various operating points.

The unrecuperated results with pressure drop added show an interesting trend. The LTT configuration is not affected much by pressure drop, while the HTT is negatively influenced by it. It can be concluded from Fig. 9 that, compared to the HTT configuration, the unrecuperated LTT produces less power and has a lower thermal efficiency. However, the LTT's power output and efficiency is less influenced by the pressure drop introduced into the system.

3.2. With recuperator

3.2.1. Recuperated LTT results

The LTT recuperated model as specified in Section 2.6.1 was used to compare the unrecuperated results with the recuperated results. The recuperator effectiveness was chosen to be a variable to be able to observe the effect on the cycle's efficiency. As mentioned in Section 2.6, the effectiveness value was 70 %, 80 % or 90 %. In this section, the recuperated cycle's thermal efficiency and heat input is compared to the unrecuperated results, assuming no pressure losses. The results are for the optimal LTT combination, where the G25-550 with A/R = 0.92 is used as the main shaft in combination with the GBC14 as the PT. The results are visually represented on the same graph in Figs. 10–12. The power output of the PT, and the temperatures at the states as shown in Fig. 5, are also represented visually in Fig. 13.

It can be noted that the required heat input decreases significantly when a recuperator is added. According to Equation (15), one would expect the efficiency to increase when considering the heat input results (since the power output stays constant for different recuperator

Table D3
Unrecuperated HTT system (without pressure losses) results with main shaft at 92 850 rpm, power turbine shaft at 104 890 rpm and 71.43 kW heat input rate (values found from analytical model) at 87 kPa ambient pressure (using the G25-550 with A/R = 0.92 as the main shaft and GBC14 as the power turbine).

Pressure ratio	Power (W)	PT mass flow rate (kg/s)	GT mass flow rate (kg/s)	T_1 (K)	T_2 (K)	T_3 (K)	T_4 (K)	T_5 (K)
1.39	1713	0.0371	0.109	300	339.65	825.8	782.36	781.36

Table D4
G25-550 with A/R = 0.92 as a single shaft power generator (without pressure losses) at 87 kPa ambient pressure.

Pressure ratio	Power (W)	Shaft speed (RPM)	Heat input rate (W)	Mass flow rate (kg/s)	T_1 (K)	T_2 (K)	T_3 (K)	T_4 (K)
1.4	1185	83 000	63 859	0.0975	300	339.8	954.5	910.6
1.522	2088	96 000	63 859	0.119	300	349.1	857.1	796.4

Table D5
G25-550 with A/R = 0.92 as a twin shaft (two G25-550 turbines in series) power generator (without pressure losses) at 87 kPa ambient pressure, compressor pressure ratio of 1.42 and heat input rate of 63.86 kW. Note that it was not possible to run a G25-550 turbine in series with a GBC14 power turbine according to Flownex.

Power (W)	Shaft speed (both shafts) (RPM)	Pressure ratio - first turbine	Pressure ratio - second turbine	Mass flow rate (kg/s)	T_1 (K)	T_2 (K)	T_3 (K)	T_4 (K)	T_5 (K)
1101	89 000	1.29	1.09	0.08	300	349.2	1078.2	1038.3	1026.3

effectiveness values, when there is no pressure drop). The results show that the recuperator had a significant effect on the cycle efficiency. As the recuperator effectiveness is increased, the cycle efficiency is also increased (due to more heat being added).

Fig. 13-a shows that the recuperator effectiveness does not influence the power output of the PT (note that the lines are plotted together and are overlapping) and that the power output is the same as for the unrecuperated cycle. The nodal temperatures are shown in Fig. 13-b. The amount of heat added to the cold side of the recuperator is equal to the amount of heat lost from the hot side of the recuperator (assumed no heat loss to the environment). The temperature difference at the cold side of the recuperator, between nodes 2 and 3, is slightly larger than the temperature difference between nodes 5 and 6, because the average specific heat of the air is slightly lower for the cold side of the recuperator. For the LTT, it can be concluded that the recuperator effectiveness only affects the heat input into the system (when pressure losses are assumed negligible) and therefore, as the effectiveness is increased, the cycle's thermal efficiency also increases.

3.2.2. Recuperated HTT results

The HTT comparison between the recuperated and unrecuperated results is shown in Figs. 14–16, for the G25-550 with A/R = 0.92 as the main shaft in combination with the GBC14 as the PT. It is noted that the cycle efficiency of the HTT is increased from a previous maximum of 4.87 % to a maximum of 10.13 %, when a recuperator is used with 90 % effectiveness. When the effectiveness is increased, only the combustion heat input into the system is affected, meaning that the power output stays constant regardless of the effectiveness. As the effectiveness is increased, the cycle's thermal efficiency is also increased.

In comparison to the LTT, the HTT has a higher mass flow rate on the cold side of the recuperator, which affects the maximum heat transfer rate, $\dot{Q}_{max}$. As a result, the cold outlet of the recuperator (see Fig. 17-b), has a temperature that is about 155 K lower than for the LTT (see Fig. 13-b). The recuperated LTT therefore has a higher efficiency than the recuperated HTT. The results for when pressure losses are introduced are shown in the following section.

3.2.3. Effect of pressure loss in the combustion chamber and in the recuperator

The recuperated results in the previous section did not include any pressure losses, meaning that, according to Fig. 5 and Fig. 6, the pressures were previously defined as $P_2 = P_3 = P_4$ and $P_5 = P_1$. Implementing pressure loss in the recuperated model would result in different operating points as a result of the gas turbine's pressure ratio decreasing. Note that the pressure losses are specified in percentages ranging from 0 % to 4 % for each of the following components: combustion chamber, cold side of the recuperator and hot side of the recuperator. Figs. 18 and 19 show the LTT and HTT results graphically and the results are also tabulated in Tables 9 and 10. Note that only the results with a combustion outlet temperature of lower than 950 °C are presented in Figs. 18 and 19 to allow for safe operation. Also note that the cycle's power output was not affected by recuperator effectiveness but that it was affected by pressure drop (the recuperator effectiveness only affected the heat input to the cycle).

The LTT has a maximum efficiency of 13.26 % with a corresponding power output of 4.06 kW at the highest simulated compressor pressure ratio of 2.0, highest recuperator effectiveness of 90 % and at a pressure drop value of 3 % (a 3 % pressure drop in each of the recuperator sides as well as 3 % in the combustion chamber). For the same case, the HTT yields a maximum efficiency of 8.66 % with a corresponding power output of 4.97 kW. This shows that the LTT has potential for further experimental investigation, especially at higher pressure ratios where it is expected to further outperform the HTT.

For the cases mentioned above, the turbine outlet temperatures are tabulated in Table 11, together with other parameters. Assuming a 100 % water heat exchanger efficiency, the turbine exhaust temperatures (where the flow streams exhaust into the atmosphere) were used to find the maximum water heating capacity available from each turbine, which were added together to find the total maximum water heating capacity of 26.6 kW for the LTT and 52.4 kW for the HTT. The EUF for the recuperated model was calculated from the data in Table 11, using the total maximum water heating capacity, power output and combustion heat input rate. The EUF calculation for both the LTT and the HTT yielded the same energy in and out of the system (EUF = 1), verifying the recuperated model.

Figs. 20–22 illustrate how the pressure drop affects the various operating points of the LTT in more detail. It is important to note that there is an increase in efficiency (for the 90 % recuperator) as the pressure drop increases.

Both the PT and gas turbine's operating ranges are plotted on their compressor maps in Fig. 23 to see how close the operating points are to the choking/surging lines. As mentioned before, the PT's compressor is not part of the cycle, but is needed to predict the operating speed of the PT.

When a pressure loss is introduced, it is noticed that the operational line on the main shaft's compressor map moves to the left. This is because the airflow required by the turbine decreases when running at lower pressure ratios. It should be noted from Fig. 23-a that the main shaft's minimum compressor pressure ratio of 1.4 is no longer compatible for pressure losses greater than 2 %. This is because there is no turbine data available from the main shaft's turbine map at the lower turbine pressure ratios when the intended pressure drop is implemented.

Similar to the results for the LTT, Figs. 24–26 illustrate in more detail how the pressure drop affects the HTT. At the highest compressor pressure ratio, in this case 2.0, the HTT performs at its most effective level. The HTT also exhibits the highest power output at the highest pressure ratio, similar to the LTT, but suffers from a significant power and efficiency loss at higher pressure drop values. The HTT operating ranges for the different pressure losses are illustrated in Fig. 27.

In the HTT configuration, both the PT and gas turbine are affected by the pressure losses. An increase in pressure loss causes the pressure ratios of both turbines to decrease. Similar to the LTT configuration shown in Fig. 23-a, the operational line on the main shaft's compressor map in Fig. 27-a moves to the left (a decrease in mass flow rate at the same compressor pressure ratio, or an increase in pressure ratio at the same mass flow rate) when a pressure loss is introduced, but with a greater magnitude than for the LTT. This is because the airflow required by both the turbines are decreased when running at lower pressure ratios.

3.3. Discussion

The GBC14, used as a low-temperature power turbine, combined with the G25-550 (A/R = 0.92) turbocharger as the main shaft, had the widest operating range out of the chosen LTT combinations when pressure losses were added, and was therefore chosen for further investigation. From the findings it is evident that the LTT configuration has better efficiency compared to the HTT configuration when considering recuperation and pressure losses for the simulated pressure ratios. When pressure losses were added to the models, it was found that the LTT's efficiency increased slightly, while the HTT's efficiency was negatively influenced by pressure losses. Seeing as pressure losses are inevitable in recuperators and combustion chambers, the LTT has an advantage. Since the LTT's power turbine operates at a much lower temperature as the HTT, it has another advantage. Furthermore, it is expected that the LTT should perform even better at higher pressure ratios.

It was found that the GBC14 turbocharger used as a low-temperature power turbine in a recuperated cycle could produce a maximum efficiency of 13.26 % with a corresponding power output of 4.06 kW at the highest simulated compressor pressure ratio of 2 and at a pressure drop value of 3 % (see Fig. 18). This was for the case where a recuperator with

90 % effectiveness was used and at an ambient pressure of 87 kPa. For the same case, the HTT configuration produced a maximum efficiency of 8.66 % and a power output of 4.96 kW. It should be noted that the power output for both configurations decreased as the pressure drop increased, but the HTT lost power at a much higher rate. The LTT could not operate at pressure drop values beyond 3 % due to the combustion outlet temperature being greater than 950 °C (see Fig. 18). In conclusion, the LTT proved to have better performance in this study compared to the HTT, and it can therefore be recommended for further investigation, especially at higher pressure ratios. However, the HTT outperforms the LTT when the cycle is not recuperated.

4. Conclusion and recommendations

4.1. Summary

In this paper, the authors investigated two variations of a small-scale parallel-flow microturbine. These variations included a low-temperature and high-temperature parallel-flow turbine for power generation. The parallel-flow configuration functions by maintaining system operation via the main shaft while the PT is used to generate power using only a fraction of the total air mass flow rate of the compressor. Off-the-shelf Garrett turbochargers were considered in different PT and gas turbine combinations. A total of sixteen combinations were presented. The different combinations were modelled for both the high-temperature and low-temperature concepts. The effects of adding pressure losses and a recuperator were also investigated when using the G25-550 (A/R = 0.92) as the main shaft and the GBC14 as the PT. Combinations were deemed incompatible when the compressor was undersized and could not supply the required mass flow rate to the turbines or when the combustion outlet temperature was greater than 950 °C (the assumed maximum safe operating inlet temperature).

4.2. Conclusion

- Results showed that the unrecuperated HTT outperformed the unrecuperated LTT.
- An optimal combination was found for the LTT configuration when the G25-550 (A/R = 0.92) used as the main shaft was coupled with the GBC14 as the PT.
- The recuperated LTT outperformed the HTT in terms of thermal efficiency at the simulated pressure ratios.
- Pressure losses improved the LTT's performance where the HTT was negatively influenced by it.
- Due to temperature constraints on the turbocharger, the LTT could not operate at pressure drop values greater than 3 % as shown in Fig. 18.
- However, there was still room for the LTT to operate at larger pressure ratios beyond what was simulated in this work.
- For a 90 % effective counterflow recuperator, the LTT with a pressure drop value of 3 % had a maximum efficiency of 13.26 % with a corresponding power output of 4.06 kW at a pressure ratio of 2.
- For the same case, the HTT configuration produced a maximum efficiency of 8.66 % with a power output of 5 kW.
- In conclusion, the LTT proved to be better when the cycle is recuperated. Seeing as actual recuperators and combustion chambers usually have significant pressure losses, there is potential for the LTT configuration to be further investigated experimentally.
- Furthermore, the lower turbine inlet temperature of the LTT presents a lower risk and longer lifespan when considering the method of connecting a generator to the power turbine running at high speeds.

4.3. Recommendations

Firstly, it is recommended that the system should be modelled at higher pressure ratios which could yield even better performance for the LTT. However, a simulation tool like Flownex should be applied to further investigate the optimum configurations which have been identified from this initial conceptual study in more detail (especially since there are slight deviations between the analytical and Flownex results - see Appendix C and Appendix D). Secondly, capital expenditure and payback time estimations are also recommended as well as an experimental investigation. The recuperated LTT could be implemented for affordable small-scale power generation and may be especially useful in hybrid solar-dish Brayton cycle applications. It may also be useful to integrate the LTT with a fuel cell. The effects of heat loss on components that were assumed to be negligible in this study can be investigated together with more realistic recuperator performance by coupling pressure drop and effectiveness as a function of recuperator dimensions (the method of entropy generation minimisation is recommended for optimisation). It should be noted that, in this conceptual study, recuperation was only applied on the gas turbine exhaust in order to compare the LTT with the HTT. A recommendation for future work is to also use the power turbine's exhaust for recuperation (for further comparison between the HTT and LTT). A last recommendation for future work would be to explore the performance of the parallel power turbine if it is placed between the recuperator and the combustion chamber.

Declaration of Competing Interest

The authors declare that they have no known competing financial interests or personal relationships that could have appeared to influence the work reported in this paper.

Data availability

Data will be made available on request.

Acknowledgements

The authors express their gratitude to the Renewable Energy Hub and Spokes Programme of the Department of Science and Innovation (DSI) for financial support through the UP Solar Thermal Spoke.

Appendix A. Equivalence model

Consider a turbocharger, as shown in Fig. A1, coupled to a generator/motor so that it can achieve steady state with the following conditions where $P_1 = P_4$ and $N = constant$:

$$\dot{W}_t = \dot{W}_C + \dot{W}_e \tag{A-1}$$

$$r = \frac{P_2}{P_1} = \frac{P_3}{P_4} \tag{A-2}$$

Note that the compressor and turbine are coupled since $P_2 = P_3$, $\dot{m}$ is a constant, and N is a constant. However, the compressor and the turbine do not necessarily have the same power under these conditions, which is why a generator/motor is also included. The power output, $\dot{W}_t$, of a turbocharger

acting as a power turbine (see Fig. A2) can therefore be simplified in an equivalent model as shown below:

$$\dot{W}_t = \eta_t \dot{m}(h_3 - h_{4s}) \tag{A-3}$$

$$\dot{W}_t = \eta_t \dot{m} C_p (T_3 - T_{4s}) \tag{A-4}$$

$$\dot{W}_t = \eta_t \dot{m} C_p T_3 \left[1 - \left(\frac{1}{r}\right)^{\frac{(k_g-1)}{k_g}}\right] \tag{A-5}$$

where

$$\eta_t = \eta_{t,max}\left[1 - \left(\frac{BSR - 0.6}{0.6}\right)^2\right] \tag{A-6}$$

and

$$BSR = \frac{\left(\frac{2\pi N}{60}\right)\left(\frac{d_t}{2}\right)}{\sqrt{2h_3\left(1 - (r)^{\frac{1-k_g}{k_g}}\right)}} \tag{A-7}$$

Note that the speed of the shaft, N, can be found from the compressor map in Fig. A3 because N is a constant, however, the corrected mass flow rate should be used when reading from the map as follows:

$$\dot{m}_{C,CF} = \dot{m} \bullet \frac{\sqrt{\frac{(T_1 - 273.15)\times 1.8 + 492}{545}}}{\left(\frac{P_1}{13.95\times 6894.8}\right)} \tag{A-8}$$

With this method, the turbine power can therefore be found for the conditions where $r = \frac{P_3}{P_4}$, T_3 and $\dot{m}$ are known.

Appendix B. Turbocharger properties and compatibility

See Tables B1 and B2.

Appendix C. Model verification

The results of the analytical modeling method are compared with results obtained with Flownex, an integrated CFD code with a graphical user interface. Flownex can typically be used for the design, simulation and optimisation of thermal fluid systems. A basic Flownex model was created (see Fig. C1) to simulate the unrecuperated LTT at one of the operating points found in this paper. The Flownex data input for the compressor and turbine maps was found from the compressor and turbine maps available from Garrett [33]. Garrett-corrected-flow had to be converted to actual flow and then to Flownex-corrected-flow [40]. The Flownex results presented in Tables C1 and C2 were found by simulating the G25-550 with A/R = 0.92 as the main shaft at 96 100 rpm and the GBC14 as the power turbine, at a pressure ratio of 1.4 and heat input rate of 63.86 kW for comparable results (using the same speed and heat input rate as the analytical model).

It is shown in Table C1 that the temperatures and pressures at each state in the cycle found in the Flownex model are very similar to the results found in the Python model with slight differences at the states after the combustion chamber, namely states 3 and 4.

When considering the temperature and pressure differences in Table C1 and the mass flow rates and pressure ratios in Table C2, it is clear that the Flownex operating point is similar to the operating point found from the Python model when simulating the Flownex model at the shaft speed of 96 100 rpm and heat input rate of 63.86 kW.

Appendix D. Additional Flownex results

See Tables D1–D5.

References

[1] A. De Almeida, P. Moura, N. Quaresma, Energy-efficient off-grid systems – review, Energ. Effi. 13 (2) (2019) 349–376, https://doi.org/10.1007/s12053-019-09813-y.

[2] N. Ouedraogo, Opportunities, barriers and issues with renewable energy development in Africa: a comprehensible review, Curr. Sustain./Renew. Energy Rep. 6 (2) (2019) 52–60.

[3] C.F. McDonald, C. Rodgers, The ubiquitous personal turbine – a power vision for the 21st century, J. Eng. Gas Turbines Power 124 (4) (2002) 835–844, https://doi.org/10.1115/1.1473826.

[4] G. Xiao, et al., Recuperators for micro gas turbines: a review, Appl. Energy 197 (2017) 83–99, https://doi.org/10.1016/j.apenergy.2017.03.095.

[5] K.E. Dellar, W.G. Le Roux, J.P. Meyer, Plate-style recuperator for a solar Brayton cycle using high-temperature sealant, Appl. Therm. Eng. 177 (2020), 115439.

[6] H. Li, Z. Zou, H. Li, Y. Chen, C. Fu, Thermal performance of a microchannel primary surface recuperator for portable microturbine generators: design and experimental study, Appl. Therm. Eng. 206 (2022), 118103.

[7] A. Traverso, A.F. Massaro, Optimal design of compact recuperators for microturbine application, Appl. Therm. Eng. 25 (14–15) (2005) 2054–2071.

[8] T. Choudhary, Sanjay, Thermodynamic assessment of advanced SOFC-blade cooled gas turbine hybrid cycle, Int. J. Hydrogen Energy 42 (15) (2017) 10248–10263, https://doi.org/10.1016/j.ijhydene.2017.02.178.

[9] W.G. Le Roux, A. Sciacovelli, Recuperated solar-dish Brayton cycle using turbocharger and short-term thermal storage, Sol. Energy 194 (2019) 569–580, https://doi.org/10.1016/j.solener.2019.10.081.

[10] M.A. Delavar, J. Wang, Simulation of a hybrid system of solar-microturbines in cold climate regions, Appl. Therm. Eng. 182 (2021), 116080.

[11] W.G. Le Roux, Feasibility study of a hybrid small-scale dish-mounted solar thermal Brayton cycle with cogeneration , in: Proceedings of the 16th International Heat Transfer Conference, IHTC-16, August 10–15, Beijing, China , 2018 , pp. 7929 – 7936 , https://doi.org/10.1615/IHTC16.nee.024185.

[12] M. Moya, J.C. Bruno, P. Eguia, E. Torres, I. Zamora, A. Coronas, Performance analysis of a trigeneration system based on a micro gas turbine and an air-cooled, indirect fired, ammonia-water absorption chiller, Appl. Energy 88 (2011) 4424–4440.

[13] R. Gomri, Thermal seawater desalination: possibilities of using single effect and double effect absorption heat transformer systems, Desalination 253 (1–3) (2010) 112–118.
[14] P. Iora, P. Silva, Innovative combined heat and power system based on a double shaft intercooled externally fired gas cycle, Appl. Energy 105 (2013) 108–115.
[15] K.G. Allen, Performance characteristics of packed bed thermal energy storage for solar thermal power plants, Thesis, University of Stellenbosch, 2010.
[16] G. Humbert, C. Roosendaal, J.K. Swanepoel, H. Navarro, W.G. Le Roux, A. Sciacovelli, Development of a latent heat thermal energy storage unit for the exhaust of a recuperated solar-dish Brayton cycle, Appl. Therm. Eng. 216 (2022), https://doi.org/10.1016/j.applthermaleng.2022.118994.
[17] G. Pasini, G. Lutzemberger, S. Frigo, S. Marelli, M. Ceraolo, R. Gentili, M. Capobianco, Evaluation of an electric turbo compound system for SI engines: a numerical approach, Appl. Energy 162 (2016) 527–540.
[18] D. Hong, T. Lee, Y. Jeong, Design and experimental validation of a high-speed electric turbocharger motor considering variation of the L/D ratio, IEEE Trans. Magn. 54 (11) (2018) 1–4.
[19] K. Subramaniam, W.-I. Salim, Modelling an electrically turbocharged engine and predicting the performance under steady-state engine, Int. J. Automot. Mech. Eng. 18 (4) (2021).
[20] T. Noguchi, Y. Takata, Y. Yamashita, Y. Komatsu, S. Ibaraki, 220,000-r/min, 2-kW PM motor drive for turbocharger, Electr. Eng. Jpn. (Engl. Transl. Denki Gakkai Ronbunshi) 161 (3) (2007) 31–40, https://doi.org/10.1002/eej.20408.
[21] T.W. Lee, D.K. Hong, Electrical and mechanical characteristics of a high-speed motor for electric turbochargers in relation to eccentricity, Energies 14 (11) (2021), https://doi.org/10.3390/en14113340.
[22] M.S. Lim, J.M. Kim, Y.S. Hwang, J.P. Hong, Design of an ultra-high-speed permanent-magnet motor for an electric turbocharger considering speed response characteristics, IEEE/ASME Trans. Mechatron. 22 (2) (2017) 774–784, https://doi.org/10.1109/TMECH.2016.2634160.
[23] Delta-Cosworth, Catalytic Generator - Zero Emissions Capable, 2021 [online], Available at: https://www.cosworth.com/capabilities/electrification/hybrid-solutions/catalytic-generator/> Accessed 26 September 2021.
[24] R. Keogh, 40 kW turbo-alternator hybrid-electric range extender, AHS Transformative Vertical Flight Concepts Workshop, Metis Design Corporation (MDC), 2015.
[25] S. Ibaraki, Y. Yamashita, K. Sumida, H. Ogita, Y. Jinnai, Development of the "hybrid turbo", an electrically assisted turbocharger, Mitsubishi Heavy Industries Ltd., Technical Review, Vol. 46, No. 3, 2006.
[26] W. Visser, S. Shakariyants, M. Oostveen, Development of a 3 kW microturbine for CHP applications, J. Eng. Gas Turbines Power 133 (4) (2011).
[27] D. Mills, Advances in solar thermal electricity technology, Sol. Energy 76 (1–3) (2004) 19–31.
[28] A. Pietsch, D.J. Brandes, Advanced solar Brayton space power systems, in: Proceedings of the Intersociety Energy Conversion Engineering Conference (IECEC), Los Alamitos, CA, 1989, pp. 911–916.
[29] T.A.C. Maia, J.E.M. Barros, B.J. Cardoso Filho, M.P. Porto, Experimental performance of a low cost micro-CAES generation system, Appl. Energy 182 (2016) 358–364.
[30] MTT. EnerTwin [online], 2022, Available at: https://enertwin.com/enertwin/ [Accessed 13 March 2022].
[31] T.A.C. Maia, et al., Test and simulation of an electric generator driven by a micro-turbine, Electr. Pow. Syst. Res. 147 (2017) 224–232, https://doi.org/10.1016/j.epsr.2017.02.033.
[32] B. Ssebabi, F. Dinter, J. van der Spuy, M. Schatz, Predicting the performance of a micro gas turbine under solar-hybrid operation, Energy 177 (2019) 121–135.
[33] Garrett, Performance Turbochargers - Garrett - G GT GTX GTW Series Turbo TBG [online], 2023 Available at: https://www.garrettmotion.com/racing-and-performance/performance-turbos/ [Accessed 20 July 2023].
[34] A. Rohatgi, WebPlotDigitizer, 2022, Available at: https://apps.automeris.io/wpd/ [Accessed 30 March 2022].
[35] P. Virtanen, et al., SciPy 1.0: Fundamental algorithms for scientific computing in Python, Nat. Methods 17 (2020) 261–272, https://doi.org/10.1038/s41592-019-0686-2.
[36] Y.A. Cengel, M.A. Boles, Thermodynamics: An Engineering Approach, 8th Edition, McGraw-Hill, Boston, 2015.
[37] I.H. Bell, et al., Pure and pseudo-pure fluid thermophysical property evaluation and the open-source thermophysical property library CoolProp, Ind. Eng. Chem. Res. 53 (6) (2014) 2498–2508, https://doi.org/10.1021/ie4033999.
[38] C. Borgnakke, R.E. Sonntag, Borgnakke's Fundamentals of Thermodynamics, Global edition, John Wiley & Sons, Hoboken, NJ, 2017.
[39] Y.A. Çengel, A.J. Ghajar, Heat and Mass Transfer: Fundamentals & Applications, 5th Edition, McGraw-Hill Education, New York, 2015.
[40] W.G. Le Roux, J.P. Meyer, Modeling the small-scale dish-mounted solar thermal Brayton cycle , in: AIP Conference Proceedings 1734, 060002, SolarPACES2015, 13-16 October, Cape Town, South Africa, https://doi.org/10.1063/1.4949144.